NASA TECHNICAL NOTE

NASA TN D-2473

NASA TN D-2473

HEAT-TRANSFER MEASUREMENT FOR BINARY GAS LAMINAR BOUNDARY LAYERS WITH HIGH RATES OF INJECTION

by C. C. Pappas and Arthur F. Okuno

Ames Research Center
Moffett Field, Calif.

NATIONAL AERONAUTICS AND SPACE ADMINISTRATION • WASHINGTON, D. C. • SEPTEMBER 1964

HEAT-TRANSFER MEASUREMENT FOR BINARY GAS LAMINAR BOUNDARY LAYERS WITH HIGH RATES OF INJECTION

By C. C. Pappas and Arthur F. Okuno

Ames Research Center
Moffett Field, Calif.

NATIONAL AERONAUTICS AND SPACE ADMINISTRATION

For sale by the Office of Technical Services, Department of Commerce,
Washington, D.C. 20230 -- Price $1.25

HEAT-TRANSFER MEASUREMENT FOR BINARY GAS LAMINAR BOUNDARY LAYERS WITH HIGH RATES OF INJECTION

By C. C. Pappas and Arthur F. Okuno

Ames Research Center
Moffett Field, Calif.

SUMMARY

Local values of surface heat transfer, wall temperature, and recovery factor were measured on a 15° porous cone with helium, air, and Freon-12 gas injection into the air stream. The effective Reynolds numbers were within the range of 1.4×10^{5} to 1.3×10^{6}. Air injection tests were made at the cone Mach numbers 3.66 and 4.35. Helium and Freon-12 injection tests were made at Mach number 4.34.

With air and Freon injection, the wall temperature shows a sharp rise from the laminar value at the start of transition to a peak in the transition region, then falls to the turbulent value. The peak wall temperature for one air injection test exceeded the air stream total temperature by 30° F and the coolant temperature by 184° F. With helium injection the wall temperature changed slightly at the start of transition but did not peak in the transition region.

The laminar heat-transfer coefficients with air injection agree with other experiments and with theory. The values go to zero at finite injection rates and remain near zero at higher injection rates. The recovery factor decreases uniformly with injection and agrees with theory.

With Freon injection, the heat-transfer coefficients decrease with increasing injection rate more rapidly than predicted. The values go to zero at finite injection rates and remain near zero at higher injection rates. The recovery factor with injection decreases uniformly to a value of 0.70.

For helium gas injection, the Stanton numbers initially increase to 1.19 times the zero injection value and then fall off with increased injection to approach the theoretical value. The rise in heat-transfer coefficient occurs at the lower Reynolds numbers of the test and decreases with increased Reynolds numbers. At the highest Reynolds numbers the heat-transfer coefficient initially decreases from its zero injection value. The binary laminar boundary-layer theories should be reconsidered in view of these results. The recovery factor values are essentially in agreement with the theory of Baron which considers the effects of thermal diffusion.

INTRODUCTION

One of the more effective heat protection mechanisms of an ablating cooling system is the heat blockage effect which results from the efflux of gases from an ablating surface. This effect is difficult to isolate and study independently when the cooling effectiveness of an ablating material is being analyzed. The mechanism of heat blockage can be studied in detail if gases of different molecular weights are transpired through a porous surface. Although many transpiration results are available in the literature, most of the laminar boundary-layer experiments and theories consider transpiration rates less than that causing laminar separation. The motivation for the present research was therefore to determine the effects of high rates of gas injection on the heating from a laminar boundary layer to a porous surface.

It is of interest then to review some of the experimental and theoretical research which is pertinent to the present study. A general review of some theoretical results considering various injection gases is presented in reference 1, and procedures (based on the ratio of molecular weights of the injected gas to the stream gas) for correlating the reduction in heat-transfer coefficient are presented. Baron (ref. 2) has included the effects of thermal and concentration diffusion in the laminar boundary-layer equations to account for previous discrepancies between the measured and theoretical recovery factor values with helium injection. Apparent agreement between theory and experiment is noted by Baron for the heat-transfer coefficients for helium injection; and for air injection, agreement is noted for both heat-transfer coefficient and for recovery factor. Hurley (ref. 3) considers the effects of injecting various gases into the laminar boundary layer at a plane stagnation region and obtains results which differ significantly from the relative heat-transfer reduction of the gases presented in reference 1. Also, Hurley finds that at low rates of hydrogen and helium injection the heat-transfer coefficient initially increases above the zero injection value; this result was not found in previous theoretical studies. Therefore, there is some doubt the methods can predict the relative effectiveness of injection gases of various molecular weights in reducing the heat transfer from a laminar boundary layer.

In the present tests the light gas helium, air, and the heavy gas Freon-12 were injected into a laminar boundary layer on a sharp cone in a supersonic air stream. The results of these and other experiments as well as theory were used to check the relative effectiveness of the various gases in reducing the heat-transfer coefficient. The boundary-layer recovery factor is compared with theory and previous experiments. Finally, the behavior of both the heat-transfer coefficient and recovery factor at high injection rates was studied in the region beyond the theoretical separation point where boundary-layer theories do not apply.

NOMENCLATURE

A	circumferential area corresponding to unit length of cone ray at each exterior thermocouple location
$\frac{A}{A_n}$	equivalent cylinder area ratio, peripheral cone area to nozzle area at thermocouple location
B_1, B_2	constants in equations (A3) and (A4)
c_h	local heat-transfer Stanton number, $\frac{h}{(\rho u c_p)_c}$
c_p	specific heat
D	diameter
F	injection mass-flow ratio normal to surface, $\frac{\rho_w v_w}{\rho_c u_c}$
h	local heat-transfer coefficient, $q = h(T_r - T_w)$
k	thermal conductivity
M	Mach number
M_c	cone Mach number, inviscid flow surface value
Pr	Prandtl number, $\frac{\mu c_p}{k}$
q	local heat-transfer rate to the wall
r	temperature recovery factor, $\frac{T_r - T_c}{T_t - T_c}$
R_c	local Reynolds number based on length of cone ray, $\frac{u_c \rho_c s}{\mu_c}$
s	distance along cone ray from tip
s_o	effective length of nonporous region of cone
T	temperature
T_i	indicated temperature
t	thickness of porous cone wall
u	velocity component parallel to cone surface or in stream direction
v	velocity component normal to cone surface

$(\rho u)_i$	mass flow of coolant past internal thermocouple corresponding to ith thermocouple
ϵ	total hemispherical emissivity
μ	viscosity of gas
ρ	density of gas
σ	Stefan-Boltzmann radiation constant
Φ	radiation form factor

Subscripts

c	cone condition, inviscid flow value at cone surface
f	evaluated at internal film temperature, $T_f = \frac{1}{2}(T_g + T_i)$
g	internal coolant value
n	wind-tunnel nozzle surface condition
o	zero injection condition
r	adiabatic recovery condition
t	stagnation condition of stream
w	cone surface condition

DESCRIPTION OF TEST EQUIPMENT

The test measurements were obtained in the Ames 10-inch heat-transfer wind tunnel. Tunnel operating conditions were controlled to allow measurement of steady-state heat transfer to a porous cone model.

Cone Model

The heat-transfer model is shown in figure 1. The test model consists essentially of an outer porous stainless steel cone and an inner porous glass fiber cone frustum. The outer seamless cone was formed of sintered type 316 stainless steel. The density of the cone material is approximately 263 pounds per cubic foot. The exterior porous surface area is 0.290 square feet and the average surface thickness is 0.053 inch. Relative porosity,

indicated by the mass-flow distribution, is shown in figure 2 along the four measurement rays of the cone. A detailed description of the porosity calibration is presented in reference 4. The outer surface of the test cone was aerodynamically smooth throughout the test period. Measurements with a tracer type instrument indicated the average roughness height to be ±200 microinches.

The inner cone frustum was made of three glass fiber conical segments glued together. Each segment was made by molding and curing a mat of glass fibers treated with uncured phenolic resin. The density of the glass fiber material is about 17 lb/cu ft, and the thickness is 0.1 inch. A solid glass fiber extension, 0.026-inch thick, was glued to the cone.

The main instrumented ray A of the outer cone has eight thermocouples numbered 1 through 8 and positioned 1 inch apart along the outer surface; each of the other three equidistant rays, B, C, and D, has four thermocouples positioned 2 inches apart. Thirty-six gage (0.005-inch diameter) chromel-constantan thermocouple wire was forced through two holes drilled in a 0.043-inch-diameter nylon 101 plug. The plug was then force fitted into a hole drilled in the cone and the ends of the thermocouple wires were spot-welded flush with the surface as shown in figure 1.

Coolant thermocouples (36-gage chromel-constantan) were mounted on the surface of the inner glass fiber cone and extension. There are eight internal thermocouples corresponding to the main cone ray; they are located in a plane defined by the main ray and the cone axis and are on lines normal to the main cone ray at each of the eight external thermocouple locations. Corresponding to the last two thermocouples of the other three rays, there are similarly located internal coolant thermocouples. These coolant thermocouples are approximately 0.425-inch inside the inner surface of the steel cone. In addition, along the main ray A, there are three coolant thermocouples 1/8-inch outside the surface of the glass fiber cone on the line normal to the fifth, sixth, and seventh thermocouples and two coolant thermocouples 1/4-inch outside the surface on the line normal to the fifth and seventh thermocouples.

Grade A helium, dry air, and commercial Freon-12 were injected through the porous cone surface into the air boundary layer. Prior to entering the model, the gases were metered with rotameters and were filtered through a fibrous glass filter twice the thickness of the inner cone and denser. It is believed that no significant porosity variations were introduced in the outer cone as a result of accumulation of matter within the porous surface. The temperature of the injection gases was controlled by a parallel system of hot and cold heat exchangers. The hot side consisted of a copper coil immersed in an electrically heated water bath and the cold side of a copper coil immersed in a dry ice and acetone mixture (-110° F) or an ice bath for Freon-12 gas injection.

TEST CONDITIONS AND CALCULATION PROCEDURES

Local heat-transfer measurements were made on the test cone at the following average test conditions:

Injection gas	M_∞	M_c	T_t, ^oR	$R_c \times 10^{-6}$, 1/ft
Air	3.98	3.66	645.4	2.80
Air	4.79	4.35	744.8	2.27
Helium	4.78	4.34	749.3	2.27
Freon-12	4.78	4.34	749.8	2.25

The measurements required to determine the local heat-transfer coefficients with gas injection were the gas inlet temperature, the test cone wall temperature (or gas exit temperature), the local mass injection rate at each surface thermocouple, the standard wind-tunnel conditions of stagnation pressure and temperature, and the test section static pressure. Free-stream Mach number was obtained from the ratio of free-stream static to tunnel stagnation pressure.

Thermocouple outputs were measured and recorded. Accuracy of temperature measurement was $\pm 0.2^\circ$ F. Total time to obtain one readout of steady-state temperatures and pressures was one minute. Temperatures, injection gas flow rate, and pressures were monitored during the course of the experiment until steady-state conditions were realized. Some 5 to 10 readouts were obtained at each test condition during the steady-state period.

Shadowgraph pictures showing the cone boundary layer and shock wave were taken for each test condition. A picture for each gas injection rate at a surface temperature near the wall adiabatic condition is shown in figure 3. From these pictures one can note (1) the effective start of the laminar boundary layer (on the forward portion of cone) with injection, (2) the boundary-layer interaction with the external flow, (3) the transition of the laminar boundary layer with gas injection, and (4) the effect of gas injection on boundary-layer thickness. For these tests the prime use of the boundary-layer photographs was to determine whether the boundary layer was laminar or not, and the effective start of the laminar boundary layer with injection. Wall temperature distributions and recovery temperature values are not sufficient indicators of a laminar boundary layer with gas injection.

The use of the individual heat-transfer measurements depends on a knowledge of the basic heat balance on a surface element of the cone. The net heat convected into the surface is:

$$q = h\left(T_r - T_w\right) = -kt\left(\frac{1}{s}\frac{\partial T_w}{\partial s} + \frac{\partial^2 T_w}{\partial s^2}\right) + \frac{\epsilon\sigma\left(T_w^4 - T_n^4\right)}{1 + \frac{\epsilon A}{A_n}\left(\frac{1}{\epsilon_n} - 1\right)} + (\rho v)_w c_{p_g}(T_w - T_g) \tag{1}$$

The first term on the right is the heat transferred out of the cone surface element by conduction only in the cone ray direction; the second term is the heat radiated out of the surface assuming a concentric cylinder geometric arrangement, and the last term is the heat absorbed by the gas coolant passing through the wall where the final temperature of the coolant is considered as the outside wall temperature. For the locations of thermocouples 1 through 8, inclusive, $\partial T_w/\partial s$ and $\partial^2 T_w/\partial s^2$ were obtained directly from a smooth curve of the surface temperature distribution. In the second term, T_w is measured directly and T_n is the wind-tunnel nozzle wall temperature which in considered to be the recovery temperature for turbulent flow. The cone surface total hemispherical emissivity was measured ($\epsilon = 0.49$) and the nozzle wall emissivity, ϵ_n, was estimated to be 0.1 for a polished stainless steel surface. The most critical values in the heat balance equation are generally in the third term. The local mass flow rate $\rho_w v_w$ must be known accurately and the accuracy of measurement over a small finite area depends primarily on the uniformity of porosity of the porous wall and on the local pressure difference across it. The mass-flow measurements presented in figure 2 show quite good uniformity from thermocouples 1 to 7 for 1/2-inch-diameter circular areas of measurement. The internal temperatures of the coolant gas, T_g, are normally correctly indicated by the corresponding internal thermocouples, but for low injection rates of Freon, air, and helium, the thermocouple readings were corrected. (Some considerations applicable to the measurement of the true internal coolant temperatures are presented in appendix A.) The average temperature of internal thermocouples 5 and 6 was used as the temperature of the injection gas emanating from the glass fiber gas-distribution cone, T_g, for thermocouples 1, 2, 3, 4, 5, and 6.

The heat-transfer coefficient, h, in equation (1) was evaluated graphically from a plot of q versus T_w/T_t for each surface thermocouple. The heat transfer was usually measured at four wall temperature levels for each gas injection rate; these data defined a straight line. The stagnation temperature, T_t, was held to within a 4.1° F range for any given injection rate from test run to run. To minimize the effects of change in the total temperature on the evaluation of the heat-transfer coefficient q was plotted against T_w/T_t rather than T_w.

All the convective heat-transfer values used in this report are obtained from equation (1) including all the terms of the equation; that is, the surface conduction term, the external radiation term, and the "correction" to T_g are included in the evaluation.

It should be noted that the reference values of the Stanton number for zero injection, c_{h_o}, are based on the effective Reynolds number, R_{s-s_o}, for all injection rates of this test. The value of s_o, the distance from the cone tip to the effective start of the boundary layer with gas injection, was determined from the shadowgraph pictures. For most of the injection rates the boundary layer thickens rapidly at $s = s_o$, thereby maintaining the effective start near $s = s_o$. At very small injection rates, however, the effective start of the boundary layer can move upstream toward the tip; and with zero injection, the start of the boundary layer is at the sharp tip

of the cone. The maximum possible uncertainty in the definition of the reference c_{h_o} value is at the location of the No. 1 thermocouple ($s_1 = 2.19$ in.). The c_{h_o} value with zero injection ($s_1 - s_o = 2.19$ in.) is 0.985×10^{-3} and the reference c_{h_o} value at low injection rates ($s_1 - s_o = 0.77$ in.) is 1.66×10^{-3}. Also, the definition of the surface temperature ahead of thermocouple No. 1 is not certain and the porosity of the surface varies in the region ahead of the thermocouple; both factors add some uncertainty to the values of heat transfer at this location.

The recovery temperature is defined as the wall temperature for the condition of zero convective heat transfer to the wall. For very low values of convective heat transfer for the laminar and transitional boundary layer, the effect of the various terms in equation (1) can markedly change the recovery temperature value. The recovery factor is reported whenever it was adequately defined.

PRESENTATION OF BASIC RESULTS

Wall-Temperature Distributions

The behavior of the porous wall temperature in the laminar and transitional boundary-layer region with gas injection is presented in figures 4, 5, 6, and 7. On every figure, corresponding to each wall-temperature level, there are presented the temperature of the coolant gas and the total temperature of the air stream. For air injection at both $M_c = 3.66$ and 4.34 (figs. 4 and 5), the wall temperature starts to rise at the beginning of transition, peaks in the transitional region, then falls off to the level expected for a turbulent boundary layer. The maximum rise in temperature decreases with increased injection.

For the test condition shown in figure 5(b), the wall temperature along ray B in the transition region exceeded the total temperature of the air stream by 30° F and coolant temperature by 184° F. Comparable high temperatures were measured along ray C. This could imply that energy separation occurred in the transitional region of the boundary layer to cause the rise in wall temperature. For Freon injection the wall temperature behaves similarly to that with air injection, but in no case did the wall temperature exceed the total temperature of the air stream. The variation in porous wall temperature along the cone for both air and Freon injection is a good indicator of boundary-layer transition. For low helium injection rates, the wall temperature variation along the cone changes slightly at the beginning of transition but does not peak in the transitional region. For the higher helium injection rates, the temperature distribution is quite uniform all along the cone from the laminar through the transitional to the turbulent boundary-layer region. Thus, for helium flow the temperature distribution, and, in fact, the recovery temperature are not good indicators of transition location.

Heat Transfer and Recovery Factor - Laminar Boundary Layer

The main effort in this experimental program was to obtain heat-transfer measurements in the laminar boundary layer with gas injection and especially at high rates of injection. For the high injection rates the heat-transfer coefficients are small and the recovery temperature somewhat difficult to obtain; also, the boundary layer tends to trip, thus limiting the extent of the laminar boundary layer. As a consequence, only a limited number of measurements of heat-transfer coefficient and recovery temperature were obtained for the three injection gases at high injection rates where the Stanton number ratio c_h/c_{h_o} was near zero.

Air injection, $M_e = 3.66$ and 4.35.- The measured local heat-transfer coefficient, shown in figure 8 and represented as the Stanton number ratio c_h/c_{h_o}, is plotted as a function of the local injection rate F normalized with respect to c_{h_o}, the local Stanton number for zero injection. The values of c_{h_o} are calculated from the laminar boundary-layer theory of reference 5 transformed to conical flow and corresponding to the local effective Reynolds number, Mach number, and insulated wall temperature. The laminar boundary layer theory of Low (ref. 6) with air injection is used for comparison. Good agreement is obtained at both Mach numbers with Low's theory over the range of validity of the theory, that is, up to the theoretical separation point. For injection rates greater than F/c_{h_o} values of 1.59 (the theoretical separation point) the experimental value of c_h remains near zero up to injection rates of $F/c_{h_o} \approx 3.1$. The present test results agree in general with other experimental heat-transfer measurements within the limits of the injection rates of the other tests; see, for example, the comparison between theory and experiment for air injection presented by Baron (ref. 2).

Some additional heat-transfer data were obtained for the range of injection rates $3.1 < F/c_{h_o} \leq 5.6$. The Stanton number ratios c_h/c_{h_o} remained near zero but there was considerable scatter in the recovery factor values. The data were for a marginally laminar boundary layer and were not presented in the report. Shadowgraph pictures of the boundary layer did not indicate any separation or blowoff of the boundary layer at the higher injection rates, but some waviness of the boundary-layer edge was evident.

The recovery temperature as represented in terms of the recovery factor ratio, r/r_o, is presented in figure 9 as a function of the gas injection rate, F/c_{h_o}. Symbols correspond to the previous figure 8. Fairly good agreement between the present experiment and the theory is obtained up to injection rates F/c_{h_o} near 1.0; again, this agreement is in accordance with previous comparisons; see Baron's report (ref. 2). For the injection rates, F/c_{h_o}, greater than 1.0 the present experimental recovery factors show considerable scatter; this scatter is the result of the small values of the corresponding heat-transfer coefficients.

We may conclude from the previous considerations that the present experimental heat-transfer and recovery-temperature measurements with air

injection are at least as accurate as other reported experimental results and that the present results are in agreement with theory. The air injection experiments provide a good test of the experimental setup and substantiation of the method of reduction of data which includes the use of an effective Reynolds number in defining the run of the injection boundary layer. Also, the value of the Stanton number c_h remains near zero at the high injection rates; this conclusion is at variance with some reported results appearing in the literature (ref. 7) where the convective heat-transfer ratio is considered to remain near 0.2 at high ablation rates.

Helium injection, $M_c = 4.35$.- The present heat-transfer coefficients in terms of Stanton number ratio c_h/c_{h_o} are presented as a function of the injection rate F/c_{h_o} in figure 10. Experiment shows that the heat-transfer-coefficient ratio increases at low injection rates above the zero injection value and then falls to approximately the theoretical value at the higher injection rates F/c_{h_o}. The experimental c_h/c_{h_o} value again approaches zero at the highest injection rates of this test. It is noted that for the lowest injection rate run ($F_{av} = 0.000128$, see fig. 7(a)), the heat-transfer coefficient is the least well defined because of the three-point line definition of the q vs. T_w/T_t curve and the small difference between the temperature levels; however, the increase in c_h/c_{h_o} values over 1.0 and the trend to the values over 1.0 are also indicated at higher injection rates.

The behavior of the Stanton number with injection rate depends on the length of run of the boundary layer. At the lower Reynolds numbers the Stanton number c_h initially increases from the zero injection value and then decreases with increased injection. At the highest Reynolds numbers the Stanton number decreases continuously with increasing injection. It is important to note that the choice of an effective boundary-layer Reynolds number can shift the c_h/c_{h_o} values of thermocouple 1 by a maximum factor of 1.60 in only the positive ordinate and abscissa direction from the plotted positions. The present c_{h_o} values are for $s_1 - s_o = 0.77$ inch, $s_2 - s_o = 1.77$ inches, etc., and the effective distances were based on shadowgraph pictures of the boundary layer with injection. If $s_1 - s_o = 1.0$ inch (the actual porous distance) is selected as the effective run of the boundary layer to thermocouple 1, then the shift in data points are those indicated by the arrows on the figure.

Initially it might by concluded that there is a major difference between the present experimental results and those reported in Baron's paper, but this is not the case. The c_h/c_{h_o} values reported by Baron can be interpreted - because of the considerable scatter - to trend to c_h/c_{h_o} values greater than 1.0 at the lower injection rates. The rise in present c_h/c_{h_o} values above 1.0 at the low helium injection rates is not without some theoretical foundation (see Hurley's paper, ref. 3). The difference between experiment and theory may be attributed to the imposition in the theory of boundary-layer similarity and to the calculated differences in physical properties of the helium-air mixtures in the inner portion of the boundary layer. It is noted that the Prandtl number of the helium-air mixture decreases rapidly from the air value for small concentrations of helium. A re-examination of some of the laminar boundary-layer theories at low helium

injection rates may be in order; also a definitive experiment, especially at low Reynolds numbers, to check the present experimental trends in c_h/c_{h_o} values would be desirable. The experiment would require: (1) accurate knowledge of the gas injection rates preceding and including all test stations; (2) accurate knowledge of all heat transfer to the porous surface element including convection, radiation, and conduction; (3) accurate measurement of the internal coolant gas temperature which includes a complete heat balance to the measurement device; (4) knowledge of the effective length Reynolds number with changing rates of injection; (5) visual records of whether the boundary layer is laminar or not; measurement of just temperature distribution or recovery temperature is not sufficient for helium injection.

The recovery factor ratio r/r_o for helium injection is presented in figure 11 as a function of the local injection rate F/c_{h_o}. Considerable scatter is evident in the data for this method of presentation, but the recovery temperature appears to increase with increasing injection. The present results are in essential agreement with the measurements reported by Baron. Baron's theoretical prediction of r/r_o values, obtained from reference 2 and which includes the effects of thermal diffusion, is shown on the figure. The experimental r/r_o values are generally slightly greater than the theoretical values. When the present recovery factor ratio is plotted as a function of the dimensionless injection rate F (fig. 12), the results correlate very well as a rising curve to r/r_o values of 1.2 for an F value of 0.7×10^{-3}. The increase in r/r_o value at higher injection rates to values over 1.6 may be subject to some error because of the inherent inaccuracy in measuring recovery temperature for conditions with low heat-transfer coefficients.

Freon-12 injection, $M_c = 4.35$.- Heat-transfer measurements for Freon-12 injection are shown in figure 13 for injection rate values of F/c_{h_o} greater than 1.0. The Stanton numbers trend to zero for F/c_{h_o} values near 1.8 and remain near zero up to the maximum test values of F/c_{h_o} near 2.5. The data are compared to the prediction of reference 1, and, in general, the experiment shows a greater decrease in heat-transfer coefficient. The authors are not aware of any other experimental data with which to compare the present results; suffice to say that the Stanton numbers with Freon-12 injection are in a correct position relative to the heat-transfer coefficients obtained with air injection. Some measurements were made at lower injection rates but it was not possible to change the wall temperature sufficiently to define the heat-transfer coefficient adequately. Also, at the low Freon injection rates the effective start of the injection boundary layer is difficult to ascertain from the shadowgraph pictures.

The recovery factors measured with Freon-12 injection are presented in figure 14. The recovery factor ratio decreases with increasing injection to a value near 0.85 for an injection rate of $F/c_{h_o} = 1.6$. Some recovery temperatures could be defined at low injection rates and these are presented for $F/c_{h_o} < 1.0$. Even though h could not be accurately defined, the q values were near zero; therefore T_r was definable with little possible error.

Effects of Reynolds number on heat-transfer coefficient.- The heat-transfer coefficient defined in terms of the Stanton number c_h is presented

as a function of the effective Reynolds number R_{s-s_o} in figures 15 through 18. The measured Stanton numbers for each thermocouple location were plotted as a function of local injection rate and curves were drawn through the data. Stanton numbers were selected at certain injection rates, F, and are plotted versus the effective Reynolds number in the figures. The zero injection reference value of Stanton number, c_{h_o}, was obtained from reference 5. The c_h vs. R_{s-s_o} curves are limited in the lower Reynolds number range because the wind tunnel could not be operated at lower total pressures. The curves are limited in the upper R_{s-s_o} range by the start of transition and also by the fact that c_h goes to zero for finite F values with consequent rapid fall off of c_h on the logarithmic plot. The upper limit, when due to transition, may be a function of the porosity distribution, wind-tunnel characteristics, Mach number, and wall temperature for any injection gas. The Stanton numbers near zero, which were obtained at the higher injection rates, are not included on the logarithmic plots.

The heat-transfer coefficients measured in the boundary-layer transitional region are not presented because the recovery temperature is not adequately defined. The heat transfer, even though it increases in the transitional region, can be independent of the wall temperature with a consequence that recovery temperature is not defined. Stanton number and recovery temperature were measured in the turbulent boundary-layer region, but the effective Reynolds number of the turbulent boundary layer is unknown; therefore, the measured values are not presented.

The variation of Stanton number with Reynolds number for both air and Freon injection generally shows similar trends except that the magnitude of the decrease in Stanton number is dependent on the injection gas. For helium injection, at the lower Reynolds numbers, the Stanton number initially increases with injection rate and then decreases. At the higher Reynolds numbers the Stanton number, with helium injection, decreases continuously from the zero injection value. Tests should be made at low Reynolds numbers to measure the variation of the Stanton number with injection of light gases. As was noted before, the laminar boundary-layer theories of Baron and others do not show the initial increase in Stanton number; these theories should be re-examined perhaps with the idea of evaluating the effects of imposed similarity of the boundary layer and the effects of the various methods for calculating the physical properties of gas mixtures.

SUMMARY OF RESULTS

Local measurements of surface heat transfer and recovery temperature were made on a porous cone surface in a laminar boundary layer with air, helium, and Freon-12 gas injected into the air stream. The effective Reynolds numbers were within the range of 1.4×10^5 to 1.3×10^6. Air injection tests were made at cone Mach numbers 3.66 and 4.35. Helium and Freon-12 injection tests were made at Mach number 4.34. Some of the pertinent observations and results follow.

The porous wall-temperature distribution through the boundary-layer transition region showed a sharp rise from the laminar value to a peak value and a fall to the turbulent value for air and Freon-12 injection. For a test with air injection, the local wall temperature exceeded the total temperature of the air stream by 30° F and the coolant temperature by 184° F. This high wall temperature may be a result of energy separation in the boundary layer in the region of transition.

For low rates of helium injection, the wall temperature changed slightly at the start of transition but did not peak in the transition region. At the higher rates of helium injection the wall temperature was essentially uniform all along the cone.

For air injection, the laminar boundary-layer values of the Stanton number ratio, c_h/c_{h_o}, agreed with other experiments and with theory. The c_h/c_{h_o} values went to zero at a finite injection rate, F/c_{h_o}, and remained near zero at higher injection rates. The recovery factor values, r/r_o, were in agreement with other experiments and with theory.

For Freon-12 injection, the experimental c_h/c_{h_o} values were not in agreement with the predictions of reference 1. The present c_h/c_{h_o} values went to zero at a finite injection rate and remained near zero at higher injection rates. The recovery factor values, r/r_o, decreased to 0.85 for an injection rate $F/c_{h_o} = 1.6$.

For helium injection, the experimental c_h/c_{h_o} values initially increased to a maximum of 1.19 and then dropped off with increased injection F/c_{h_o} to approach the theoretical value. The rise in c_h/c_{h_o} over 1.0 occurred at the lower Reynolds numbers of the test (short run of boundary layer) and the rise decreased with increasing Reynolds number. At the higher Reynolds numbers the c_h/c_{h_o} values initially decreased from the zero injection value. The theories for a binary gas in a laminar boundary layer should be reconsidered in view of these results. The correlation of recovery factors r/r_o, with helium injection, was better when based on an injection rate F rather than F/c_{h_o}.

Ames Research Center
National Aeronautics and Space Administration
Moffett Field, Calif., July 2, 1964

APPENDIX A

INTERNAL TEMPERATURE MEASUREMENT OF INJECTION GAS

For the low rates of gas injection the forward internal thermocouples indicate a gas inlet temperature which is incorrect in that it tends to follow the external wall temperature. This indicated coolant temperature is the result of the net heat exchange to the thermocouple junction from radiative and convective heat transfer. The gas temperature, T_g, is given by the heat balance equation:

$$T_g = T_i + \frac{\epsilon_i \Phi_i \sigma}{h_i}\left[\left(\frac{T_i}{100}\right)^4 - \left(\frac{T_w}{100}\right)^4\right] \tag{A1}$$

The second term on the right must be minimized in order for the indicated temperature T_i to correctly represent the gas temperature. For the present tests T_g was taken to be $(1/2)(T_5 + T_6)$ for the following reasons: (1) Analysis of the internal flow shows that $\epsilon_i \Phi_i \sigma / h_i$ is a minimum for internal thermocouple 5 and near minimum for thermocouple 6, because $(\rho u)_5$ is maximum and $\epsilon_5 \Phi_5$ a minimum, and $(\rho u)_6$ a near maximum and $\epsilon_6 \Phi_6$ a minimum; (2) the temperature difference, $T_i^4 - T_w^4$, is usually a near minimum except when the wall temperature is increased by effects of transition for air and Freon injection.

The model design and imposed test conditions did not allow an independent measure of either the radiative or convective heat transfer to the internal thermocouples. In order to check the correctness of the postulated heat exchange to the thermocouple an indirect approach was adopted. From equation (A1)

$$\frac{h_i}{\epsilon_i \Phi_i \sigma k_f Pr_f^{1/3}} = \frac{\left[\left(\frac{T_i}{100}\right)^4 - \left(\frac{T_w}{100}\right)^4\right]}{(T_g - T_i) k_f Pr_f^{1/3}} \tag{A2}$$

The convective heat-transfer coefficient for the low speed internal flow may be represented by the equation

$$\frac{h_i D_i}{k_f} = B_1 Pr_f^{1/3} \left(\frac{\rho_i u_i D_i}{\mu_f}\right)^n \tag{A3}$$

or for any internal thermocouple

$$\frac{h_i}{\epsilon_i \Phi_i \sigma k_f Pr_f^{1/3}} = B_2 \left(\frac{\rho_i u_i}{\mu_f}\right)^n \tag{A4}$$

When $h_i/\epsilon_i\Phi_i\sigma k_f Pr_f^{1/3}$, as obtained from the heat-balance equation, is plotted as a function of $\rho_i u_i/\mu_f$ for all injection gases, flow rates, and internal thermocouples, and where $(T_i - T_g)$ is not too small, a consistent correlation is obtained for each thermocouple. However, the value of n for helium injection was 1.80 and for air and Freon $n = 0.77$. The consistency of the individual results indicates that the postulated heat exchange is correct, but the consequences of the change in value of n for helium flow are unknown at present. Flow Reynolds numbers $\rho_i u_i D_i/\mu_f$ are of the order of unity for all the tests so flow over the thermocouples should be laminar.

REFERENCES

1. Gross, J. F., Hartnett, J. P., Masson, D. J., and Gazley, C., Jr.: A Review of Binary Laminar Boundary Layer Characteristics. The RAND Corp., RM 2516, June 18, 1959.

2. Baron, Judson R.: Thermodynamic Coupling in Boundary Layers. ARS Journal, vol. 32, no. 7, July 1962, pp. 1053-9.

3. Hurley, D. G.: Mass Transfer Cooling in a Boundary Layer. The Aeronautical Quarterly, vol. 12, part 2, May 1961, pp. 165-188.

4. Pappas, C. C., and Okuno, Arthur F.: Measurement of Heat Transfer and Recovery Factor of a Compressible Turbulent Boundary Layer on a Sharp Cone With Foreign Gas Injection. NASA TN D-2230, 1964.

5. Chapman, Dean R., and Rubesin, Morris W.: Temperature and Velocity Profiles in the Compressible Laminar Boundary Layer With Arbitrary Distribution of Surface Temperature. Jour. Aero. Sci., vol. 16, no. 9, Sept. 1949, pp. 547-565.

6. Low, G.: The Compressible Boundary Layer With Fluid Injection. NACA TN 3404, 1955.

7. Lundell, John H., Winovich, Warren, and Wakefield, Roy M.: Simulation of Convective and Radiative Entry Heating. Advances in Hypervelocity Technique, Plenum Press, New York, 1962, pp. 729-748.

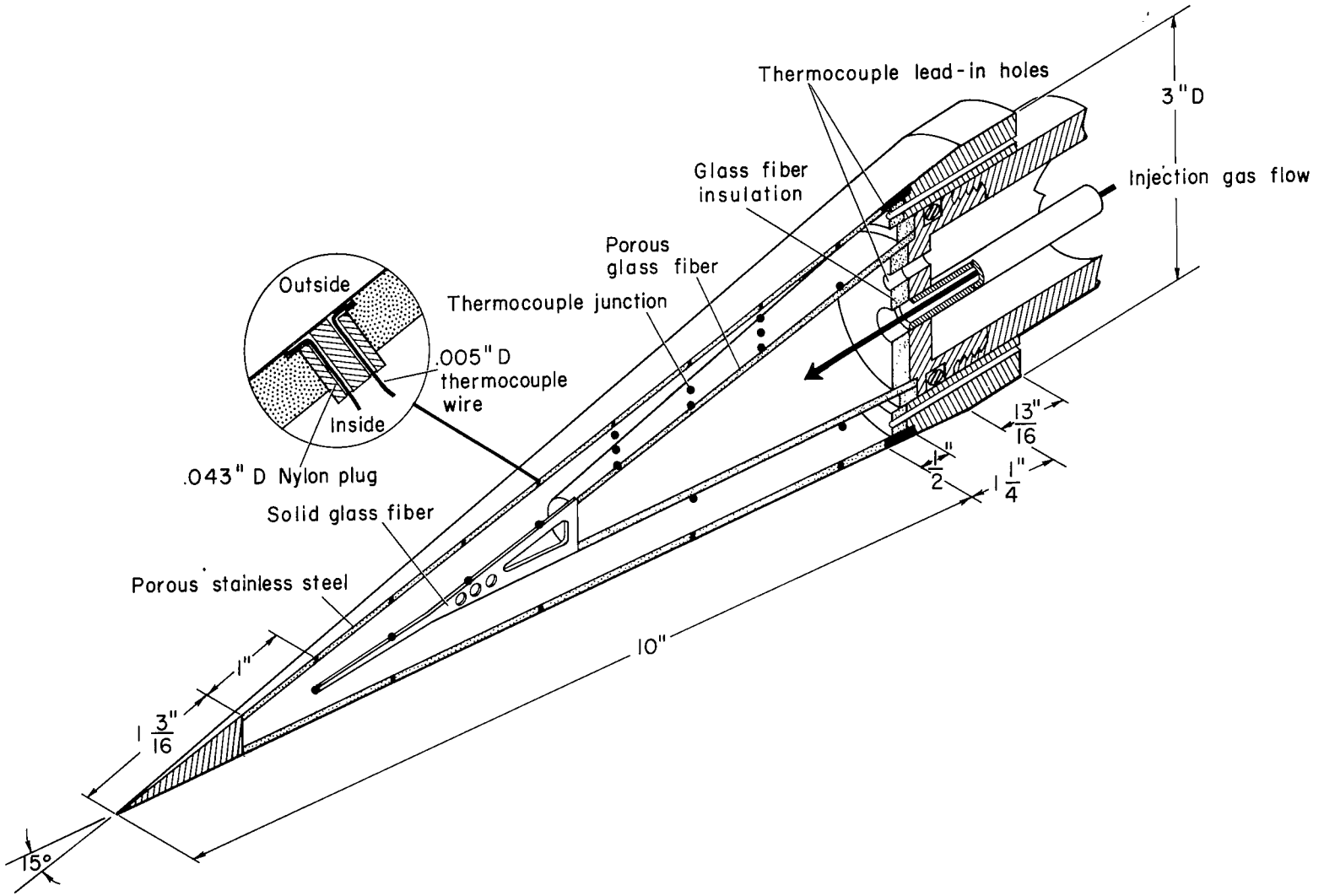

Figure 1.- Cone heat-transfer model.

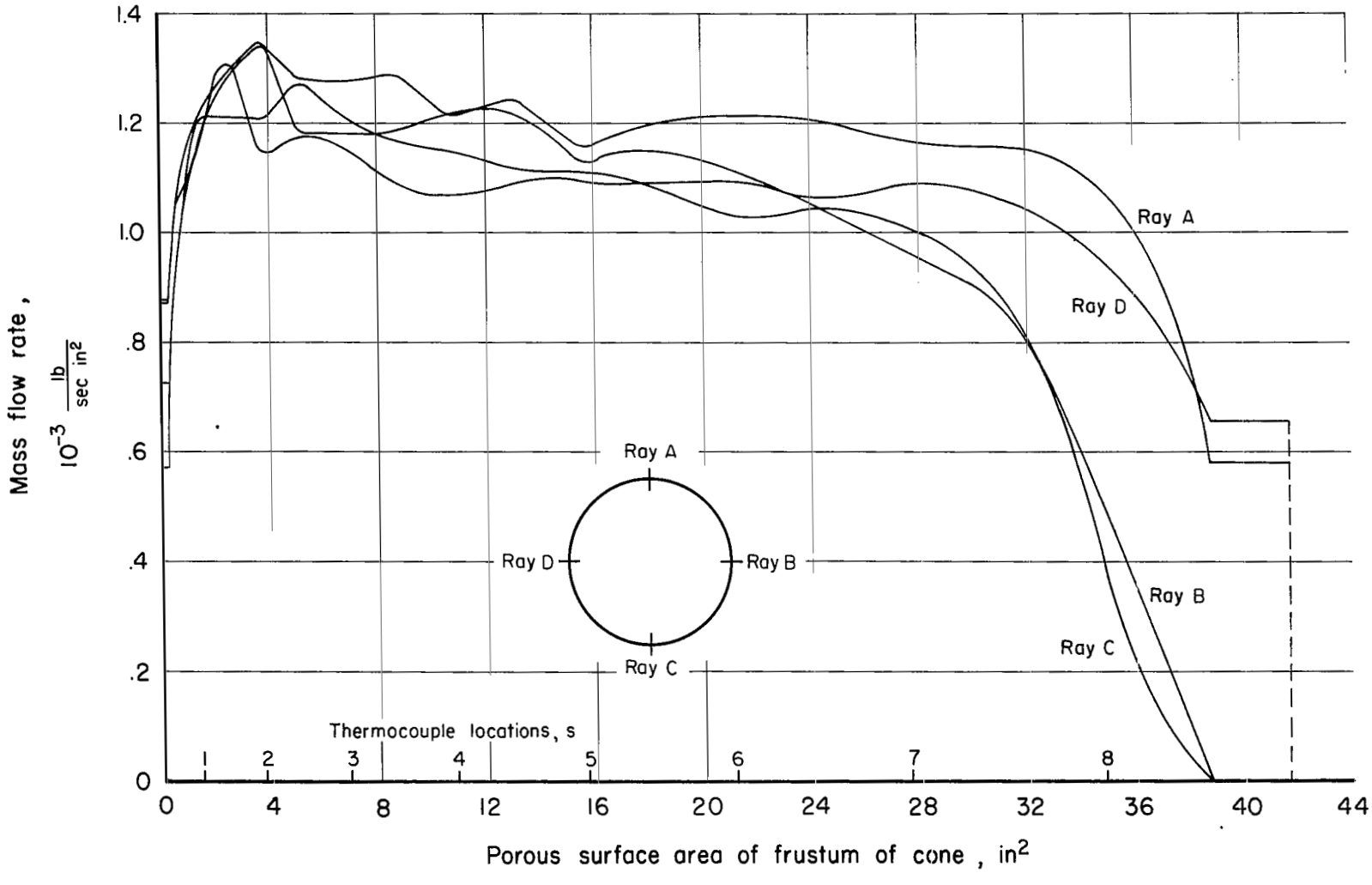

Figure 2.- Distribution of mass-flow rate through porous cone.

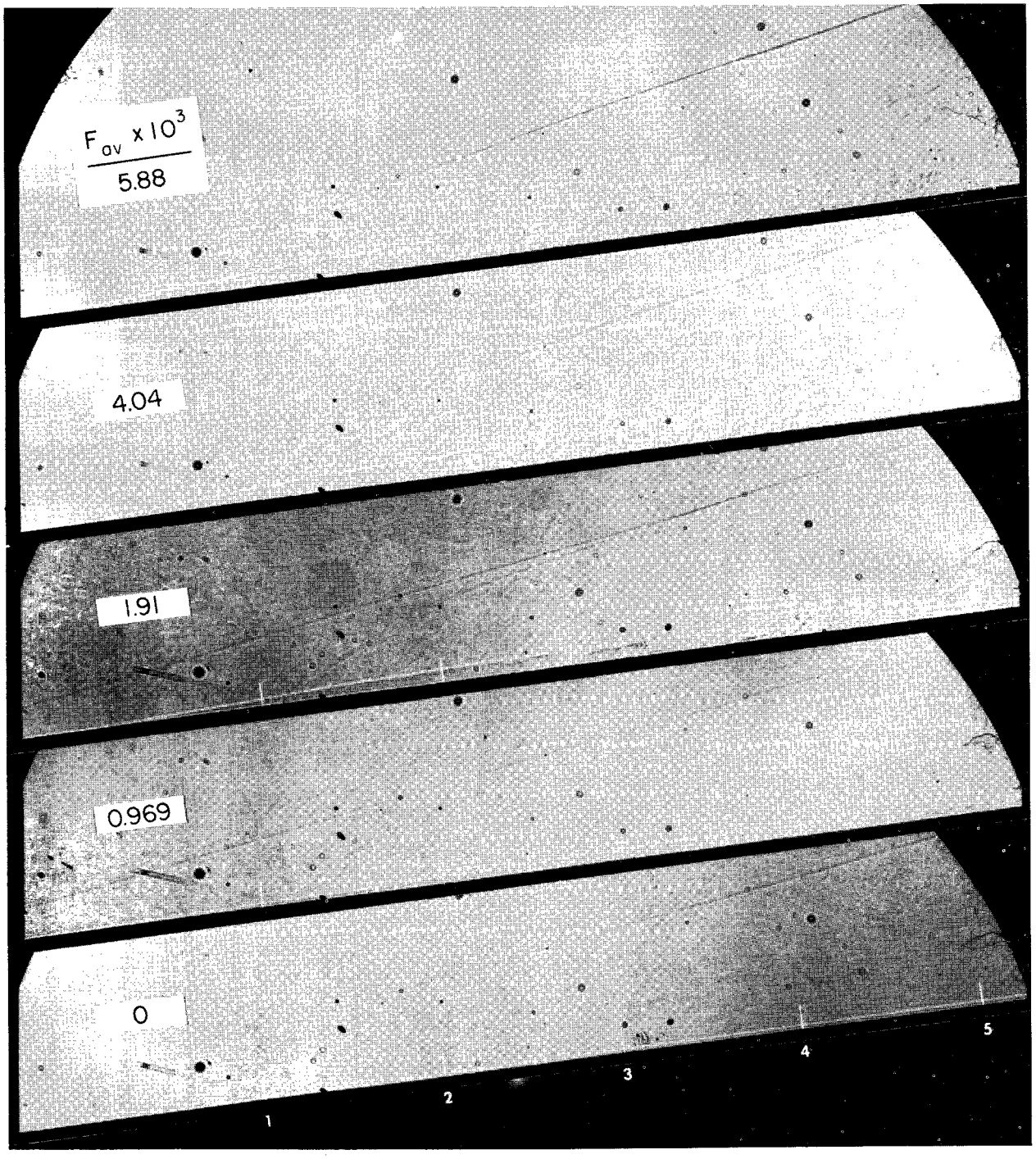

(a) Air injection; M_c = 3.66; $F_{av} \times 10^3$ = 0, 0.969, 1.91, 4.04, 5.88.

Figure 3.- Boundary-layer shadowgraphs.

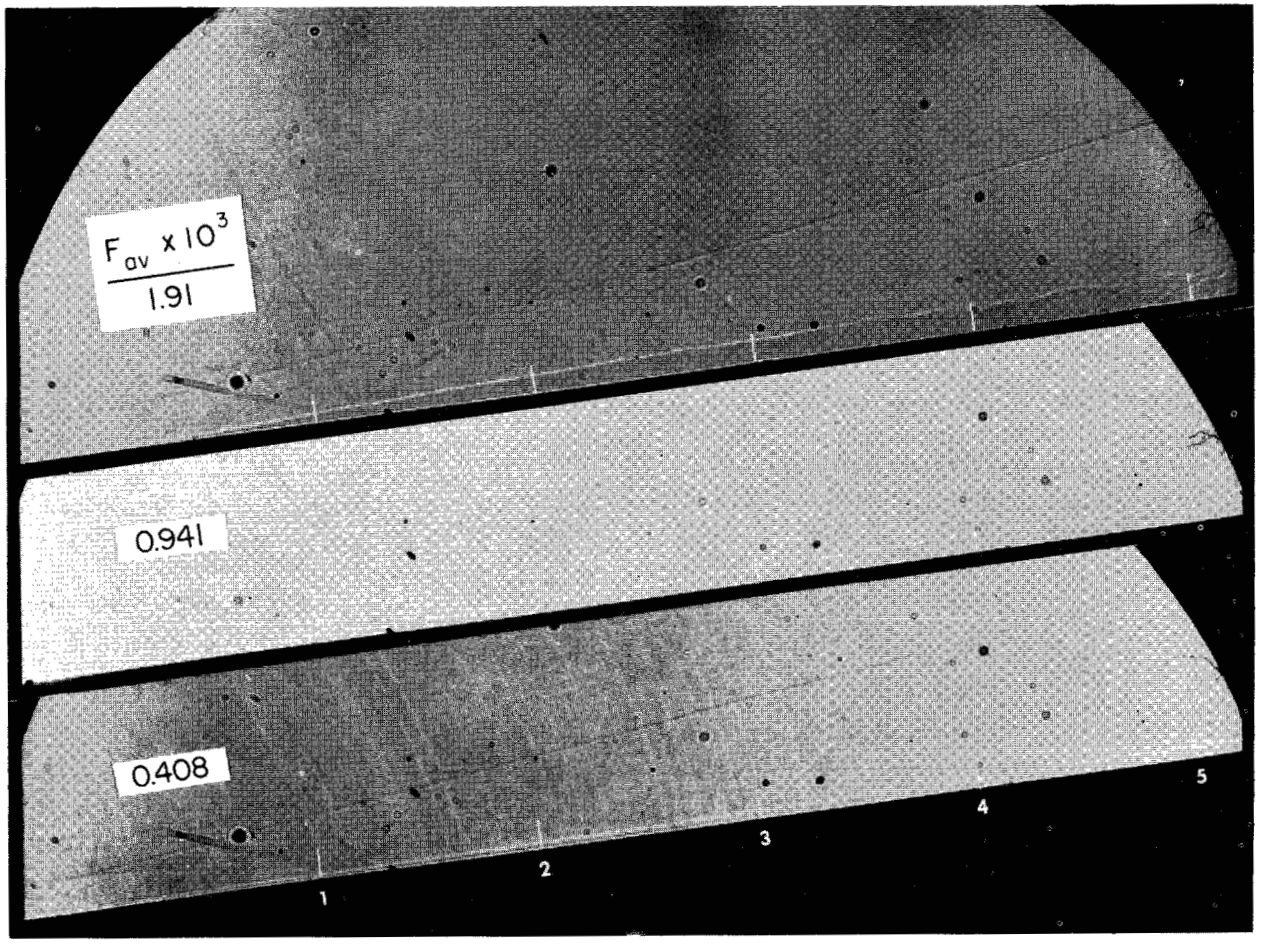

(b) Air injection; $M_c = 4.35$; $F_{av} \times 10^3 = 0.408, 0.941, 1.91$.

Figure 3.- Continued.

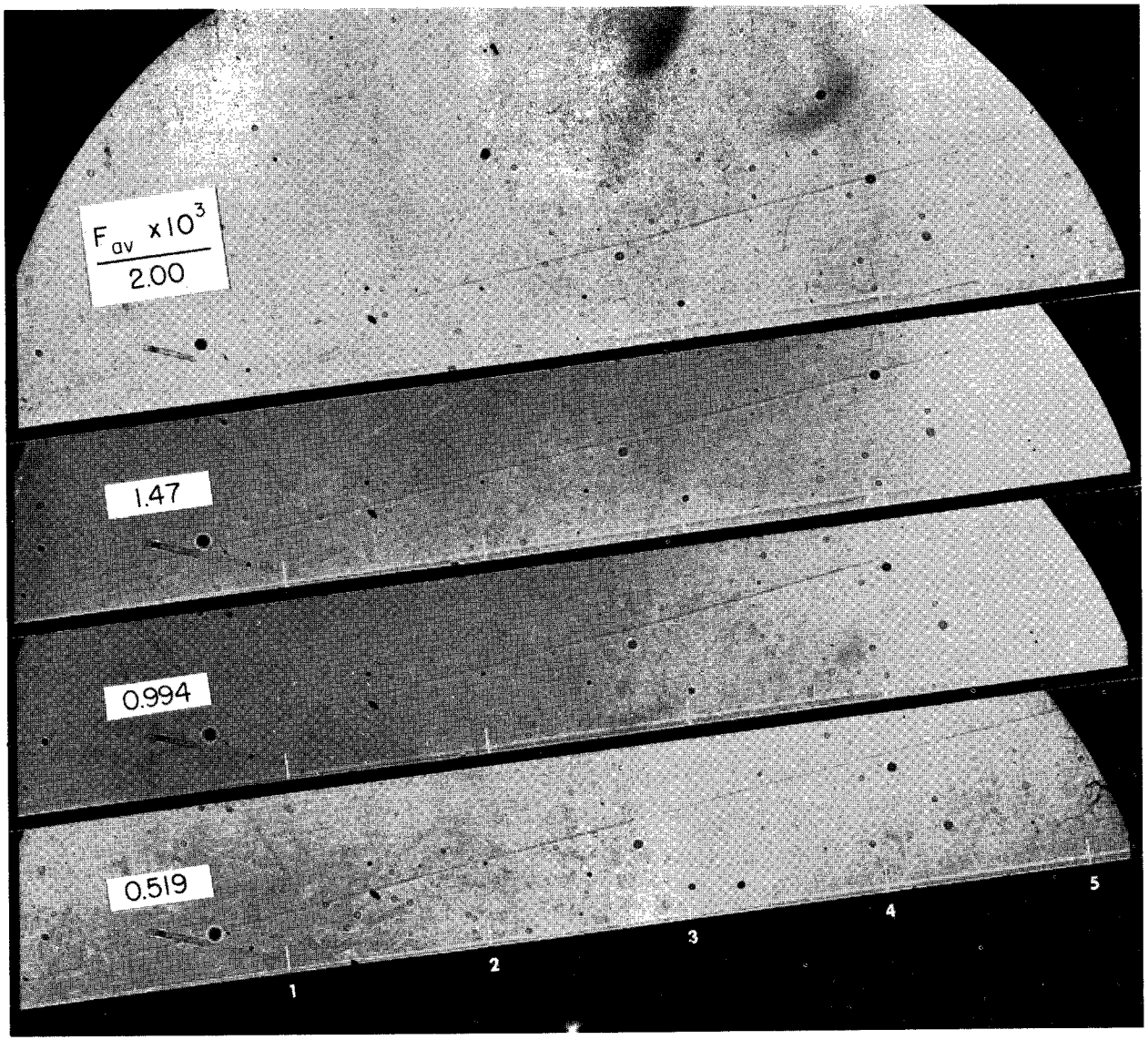

(c) Freon-12 injection; M_c = 4.34; $F_{av} \times 10^3$ = 0.519, 0.994, 1.47, 2.00.

Figure 3.- Continued.

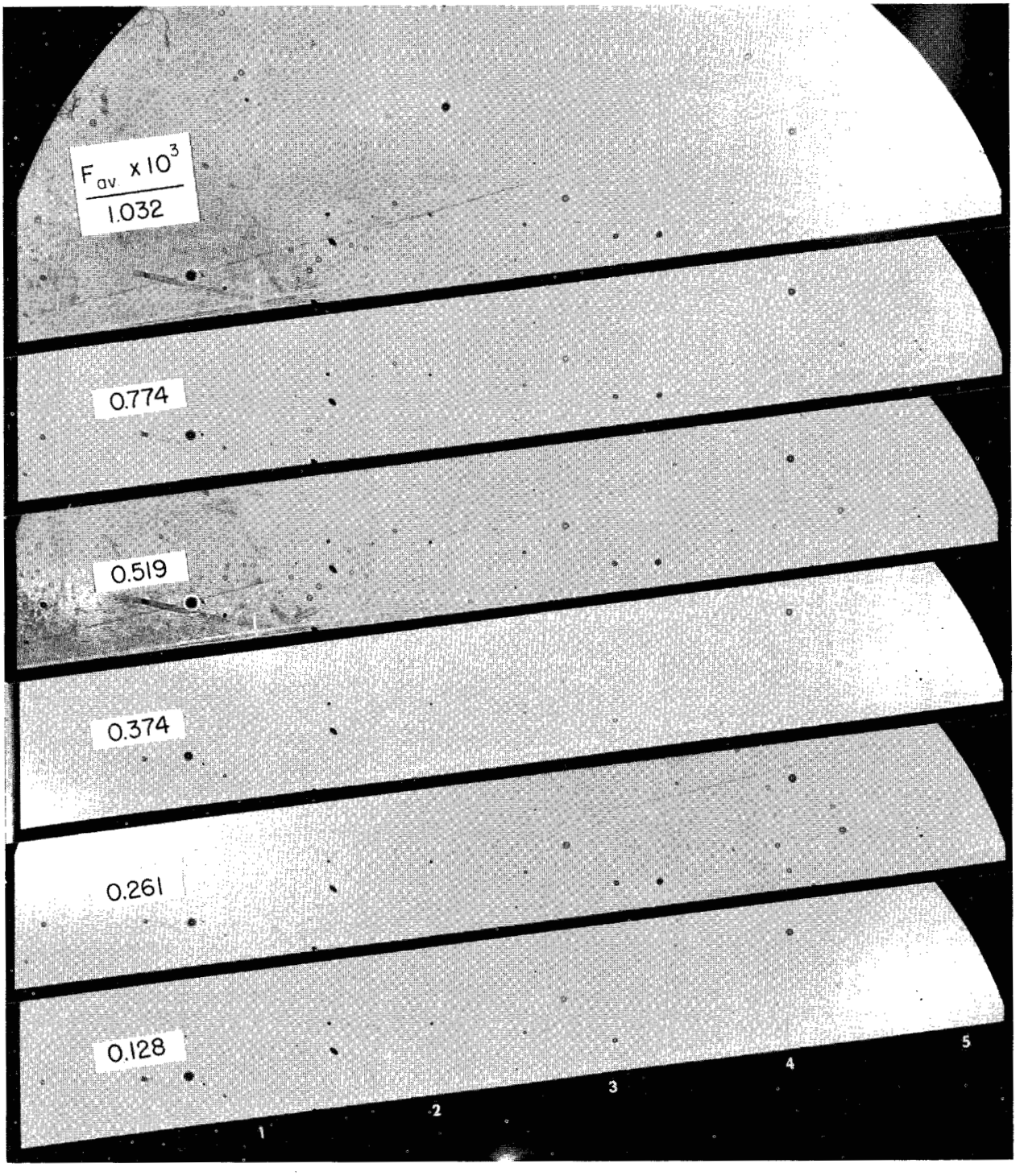

(d) Helium injection; $M_c = 4.34$; $F_{av} \times 10^3 = 0.128, 0.261, 0.374, 0.519, 0.774, 1.032$.

Figure 3.- Concluded.

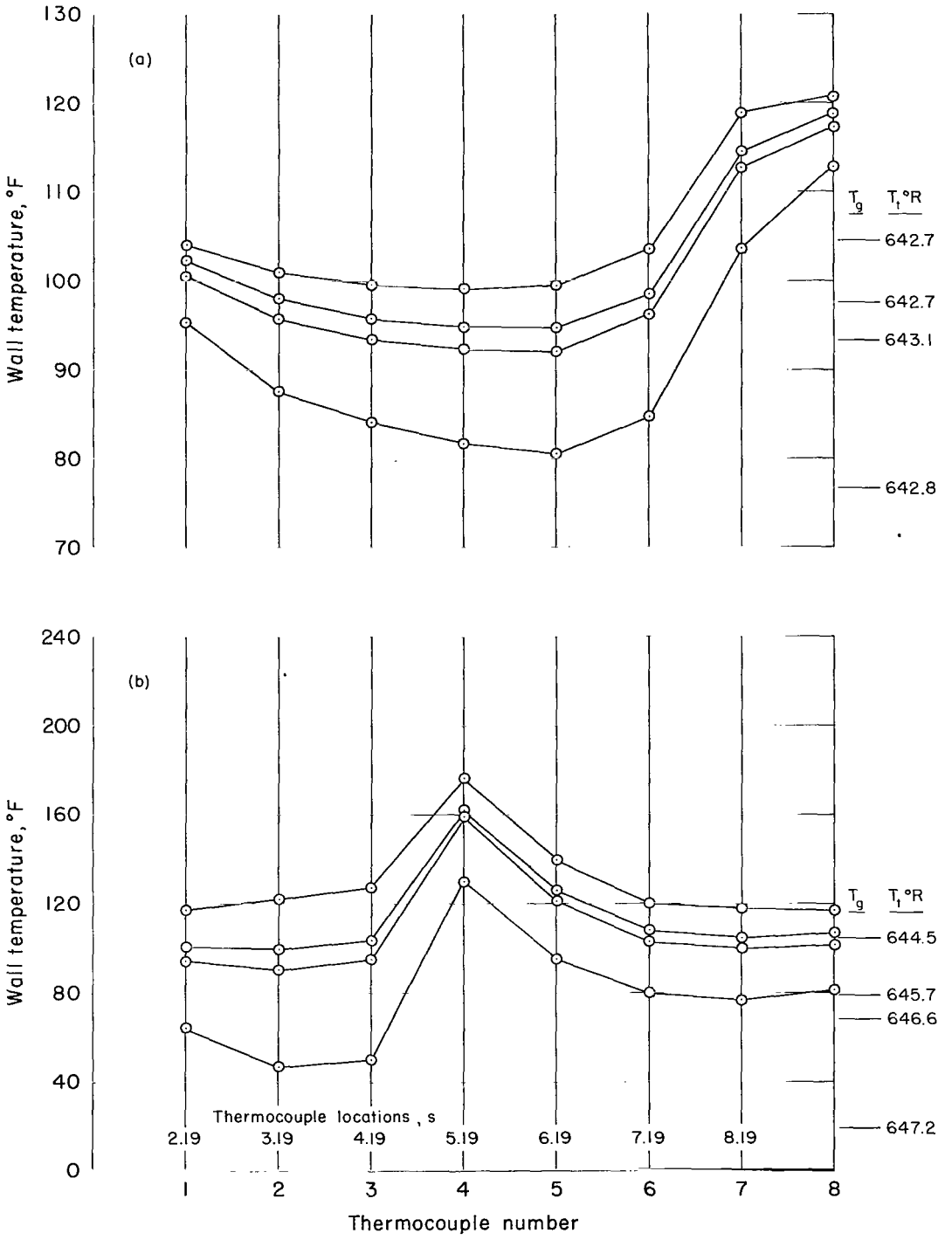

(a) $F_{av} = 0.485 \times 10^{-3}$
(b) $F_{av} = 0.969 \times 10^{-3}$

Figure 4.- Distribution of porous wall temperature; air injection; $M_c = 3.66$.

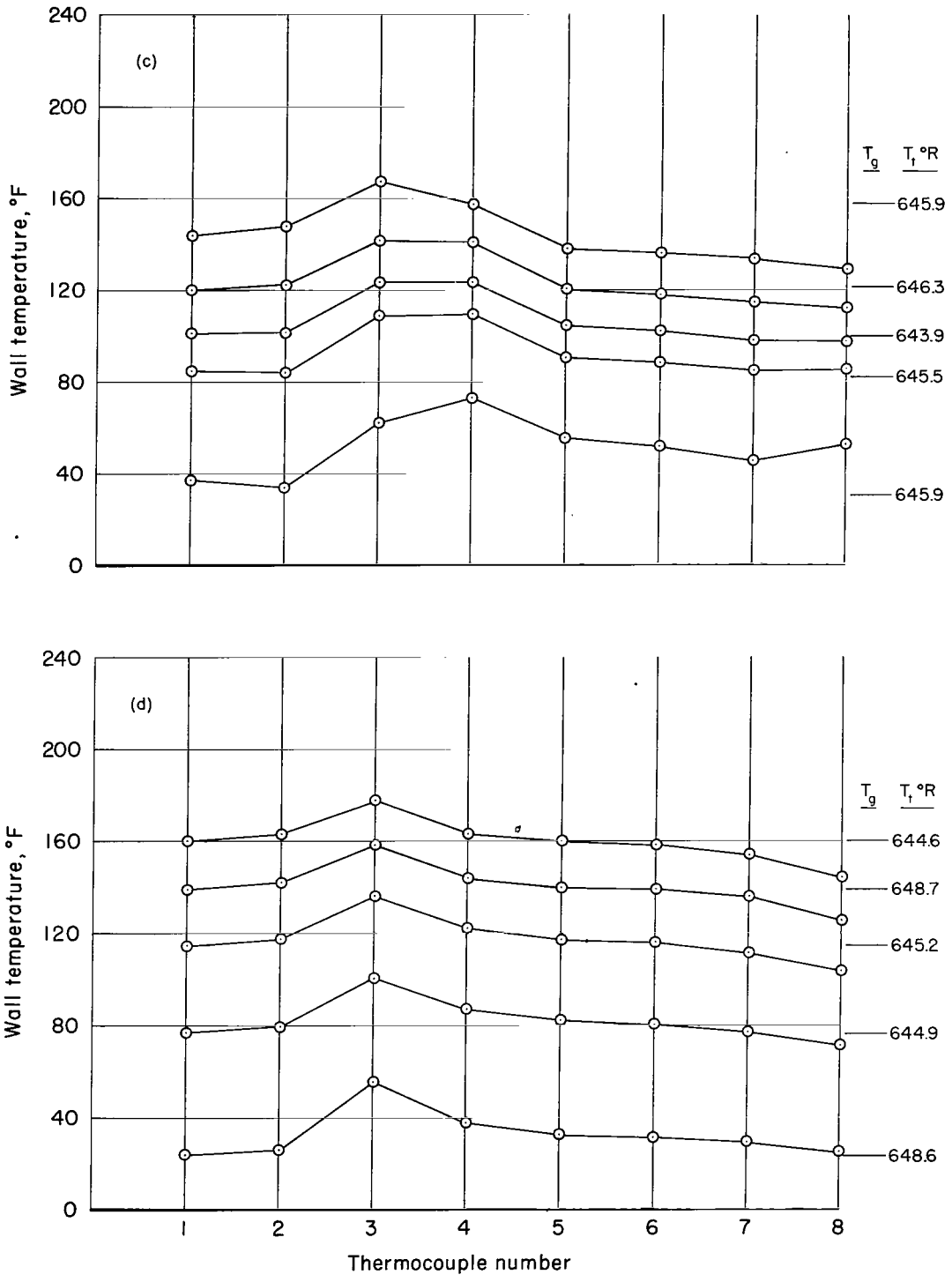

(c) $F_{av} = 1.91 \times 10^{-3}$
(d) $F_{av} = 4.04 \times 10^{-3}$

Figure 4.- Concluded.

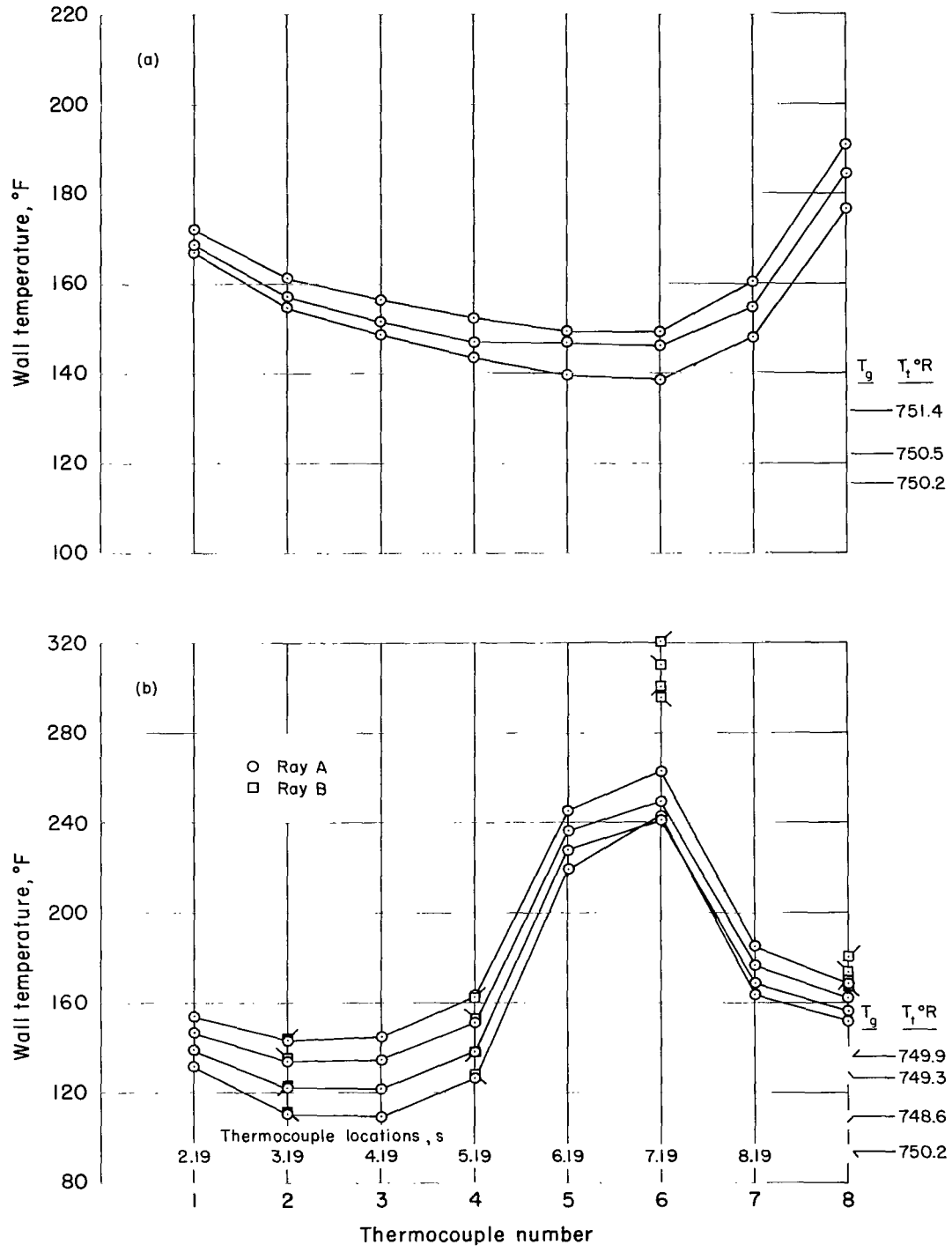

(a) $F_{av} = 0.408 \times 10^{-3}$
(b) $F_{av} = 0.941 \times 10^{-3}$

Figure 5.- Distribution of porous wall temperature; air injection; $M_c = 4.35$.

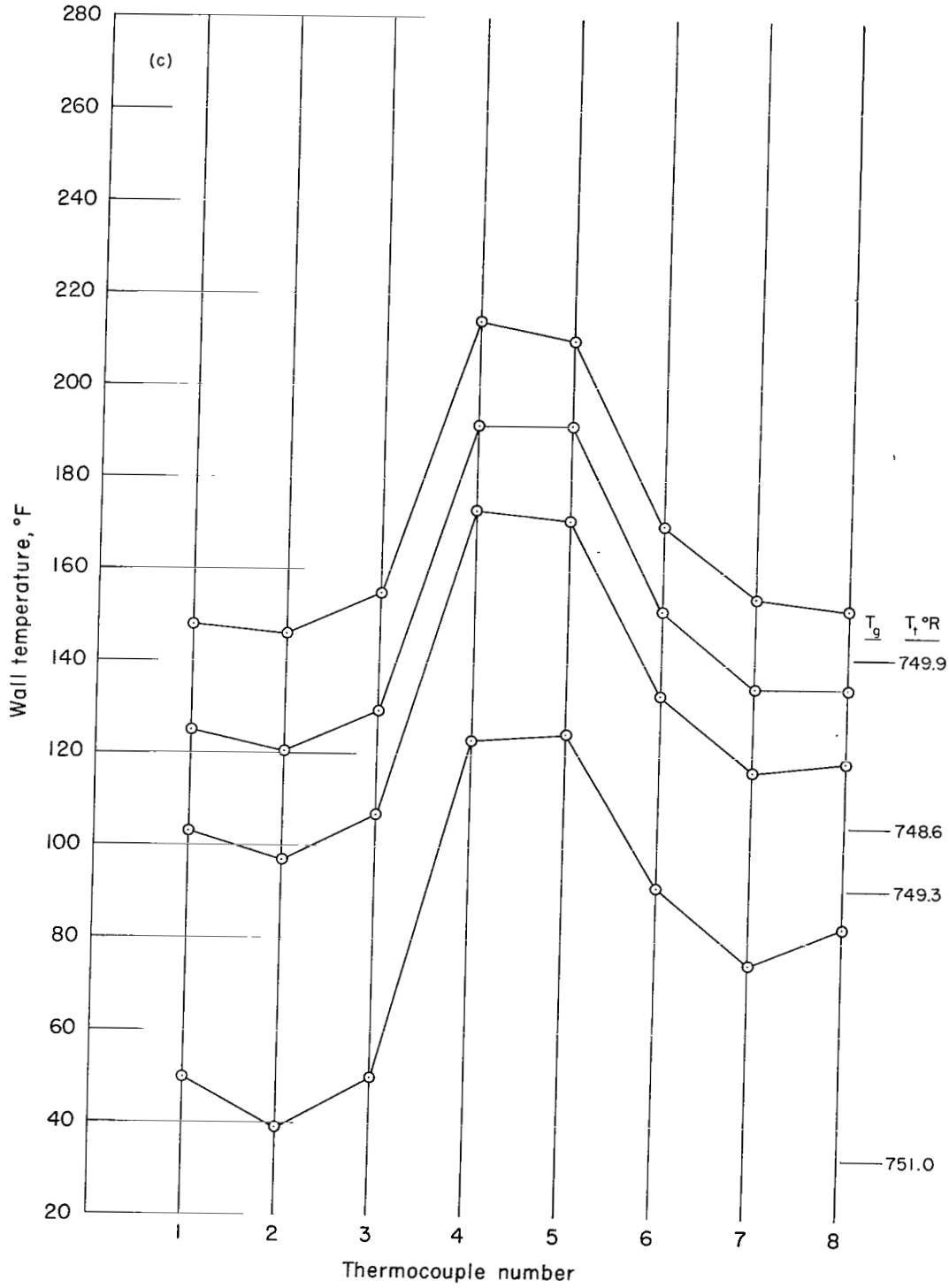

(c) $F_{av} = 1.91 \times 10^{-3}$

Figure 5.- Concluded.

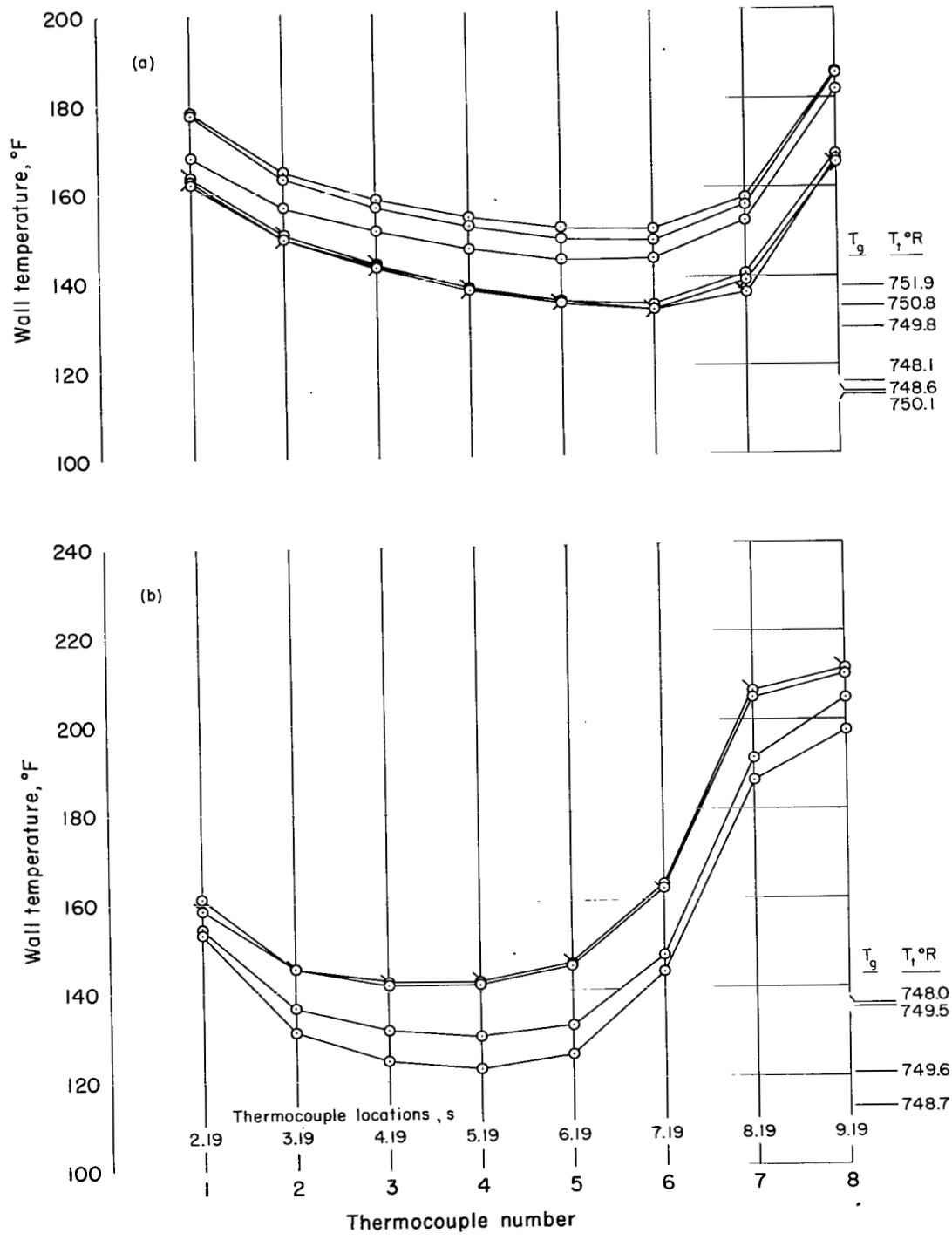

(a) $F_{av} = 0.519 \times 10^{-3}$
(b) $F_{av} = 0.994 \times 10^{-3}$

Figure 6.- Distribution of porous wall temperature; Freon-12 injection; $M_c = 4.34$.

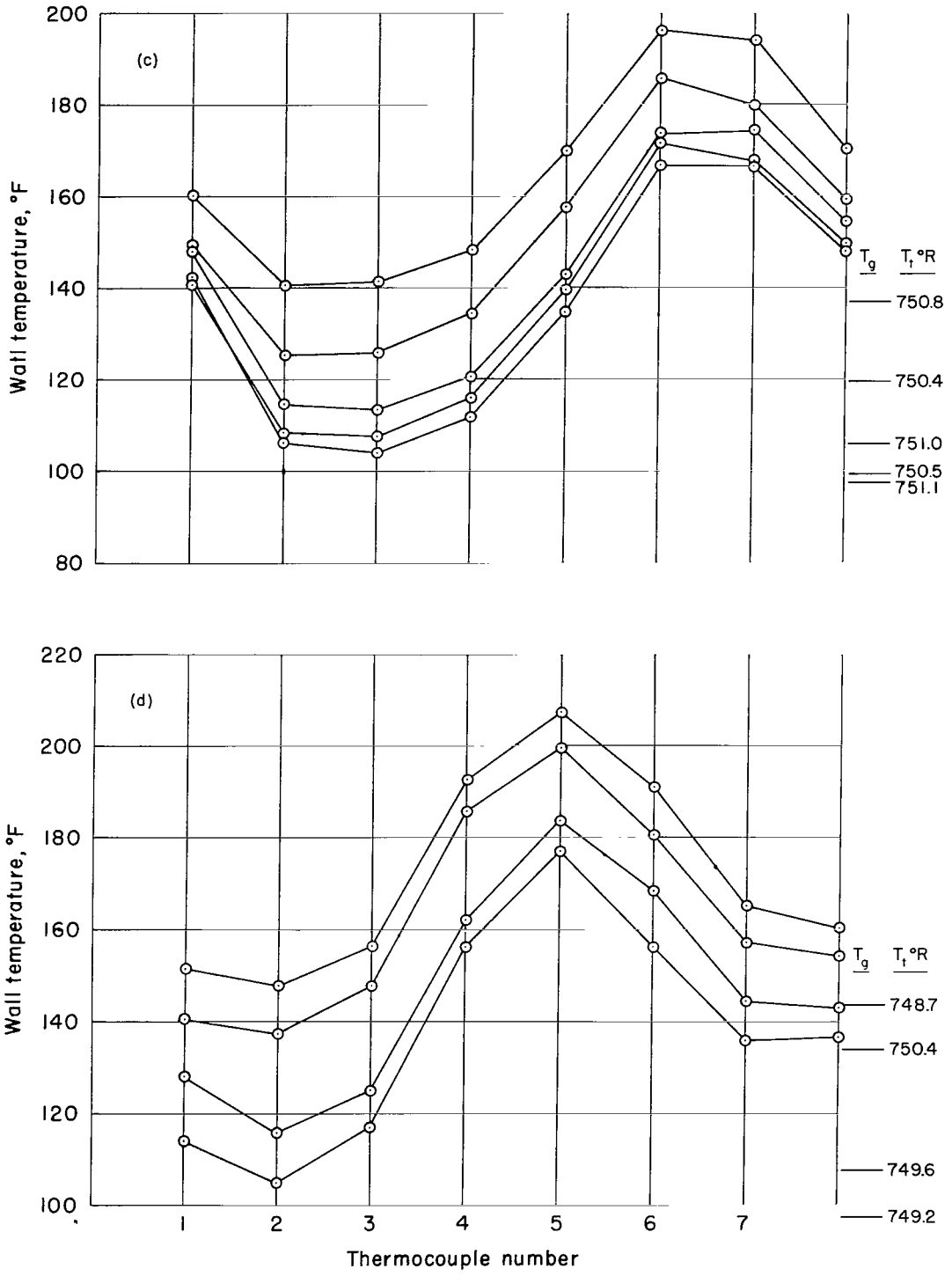

(c) $F_{av} = 1.47 \times 10^{-3}$
(d) $F_{av} = 2.00 \times 10^{-3}$

Figure 6.- Concluded.

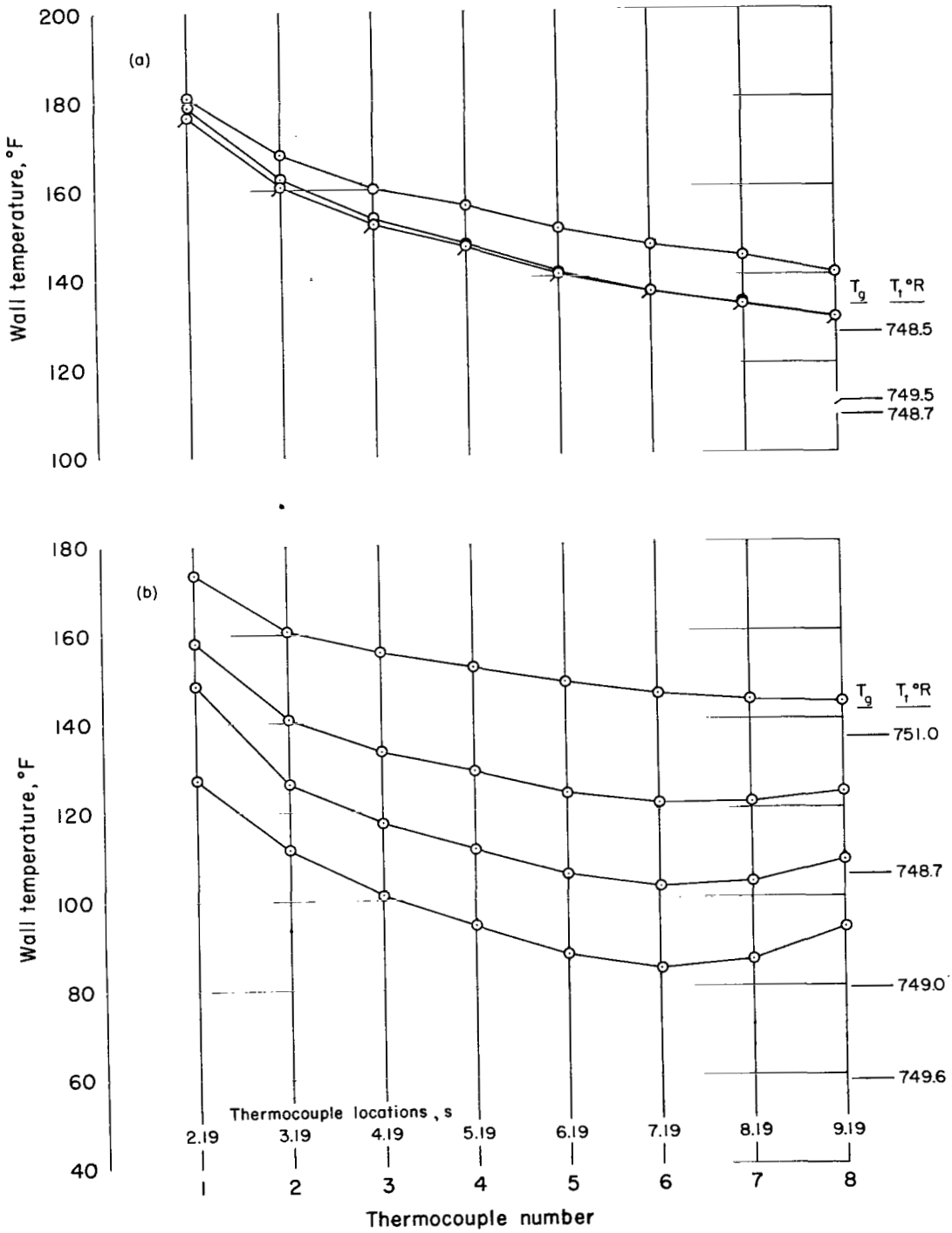

(a) $F_{av} = 0.128 \times 10^{-3}$
(b) $F_{av} = 0.261 \times 10^{-3}$

Figure 7.- Distribution of porous wall temperature; helium injection; $M_c = 4.34$.

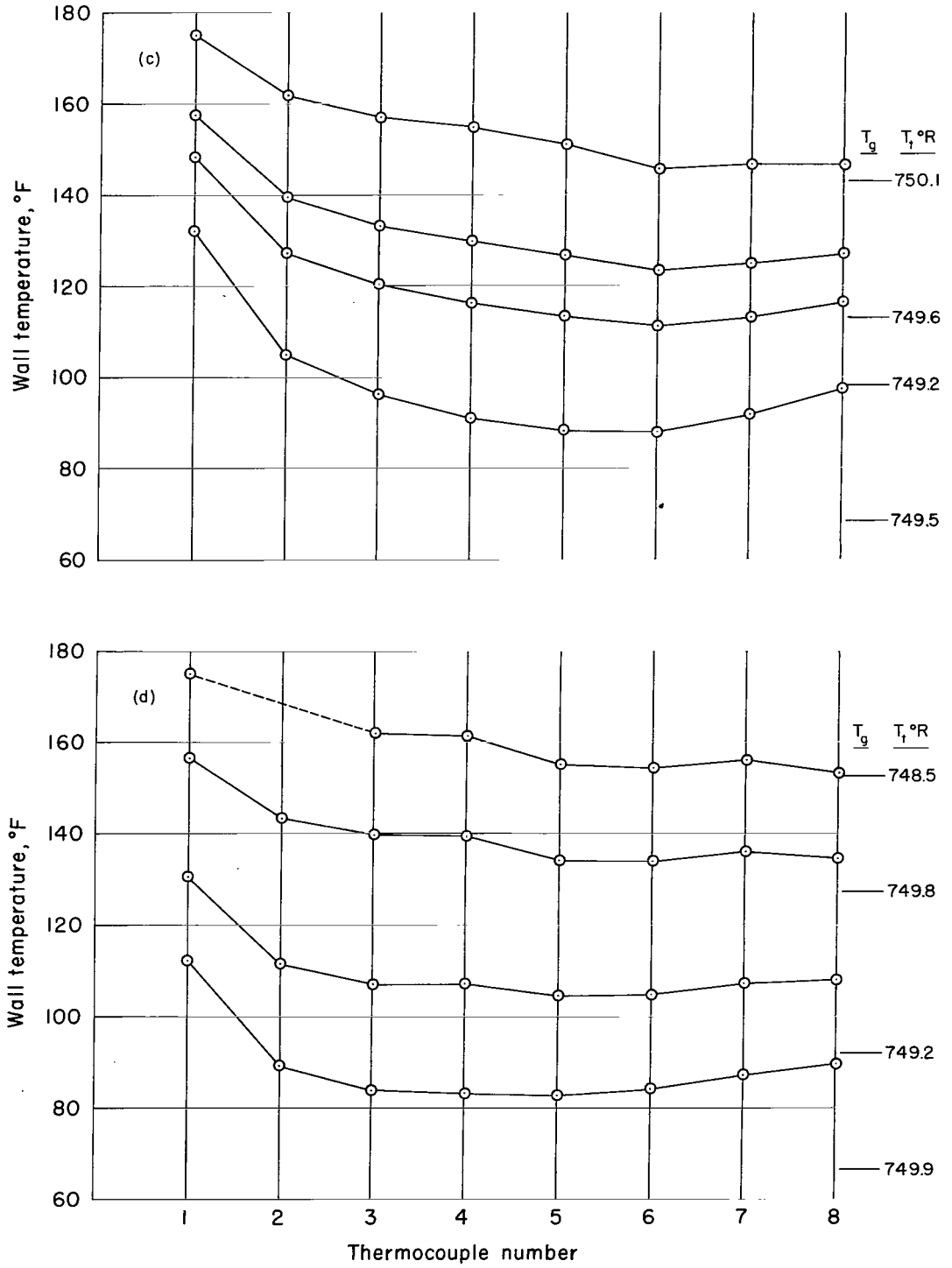

(c) $F_{av} = 0.374 \times 10^{-3}$
(d) $F_{av} = 0.519 \times 10^{-3}$

Figure 7.- Continued.

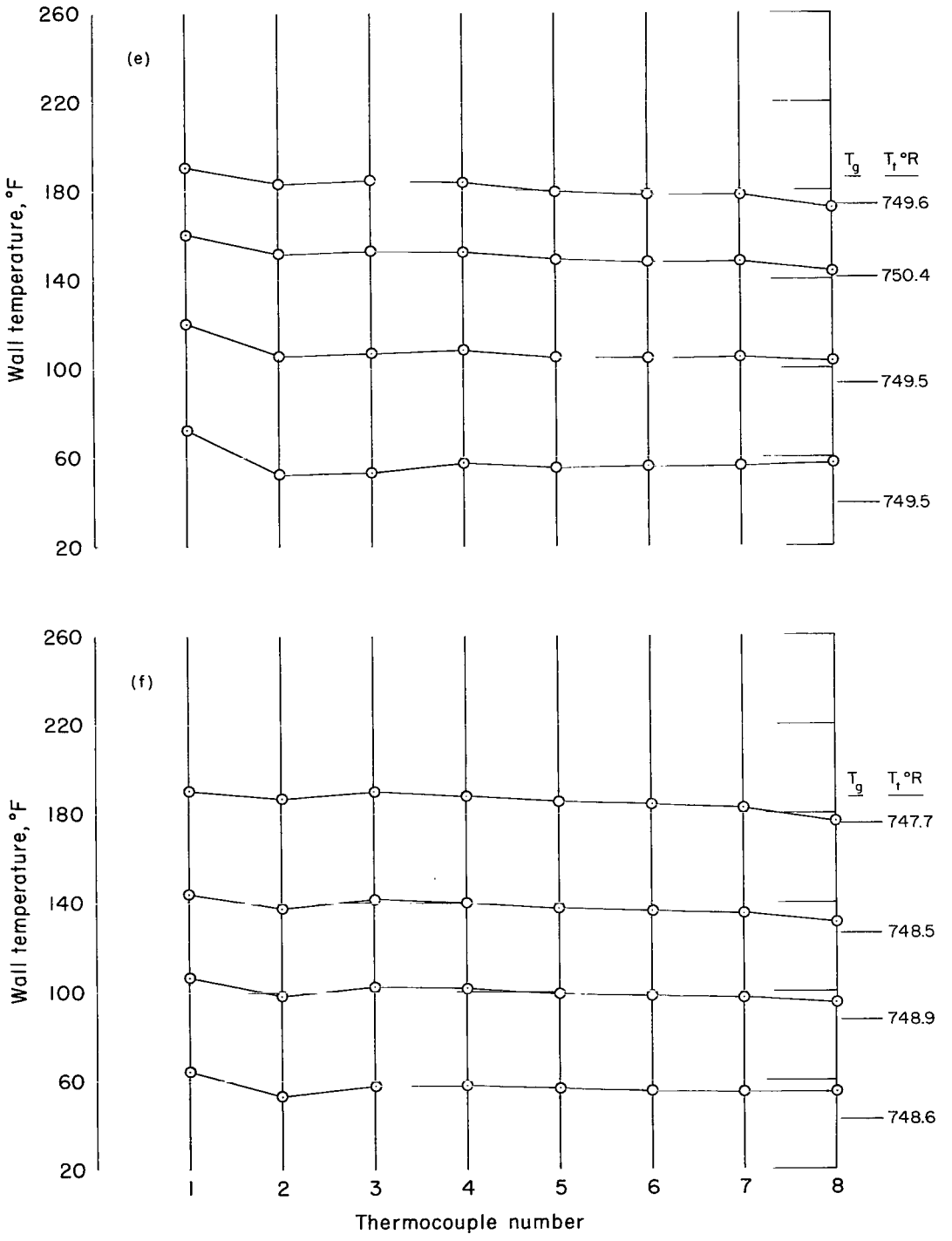

(e) $F_{av} = 0.774 \times 10^{-3}$
(f) $F_{av} = 1.032 \times 10^{-3}$

Figure 7.- Concluded.

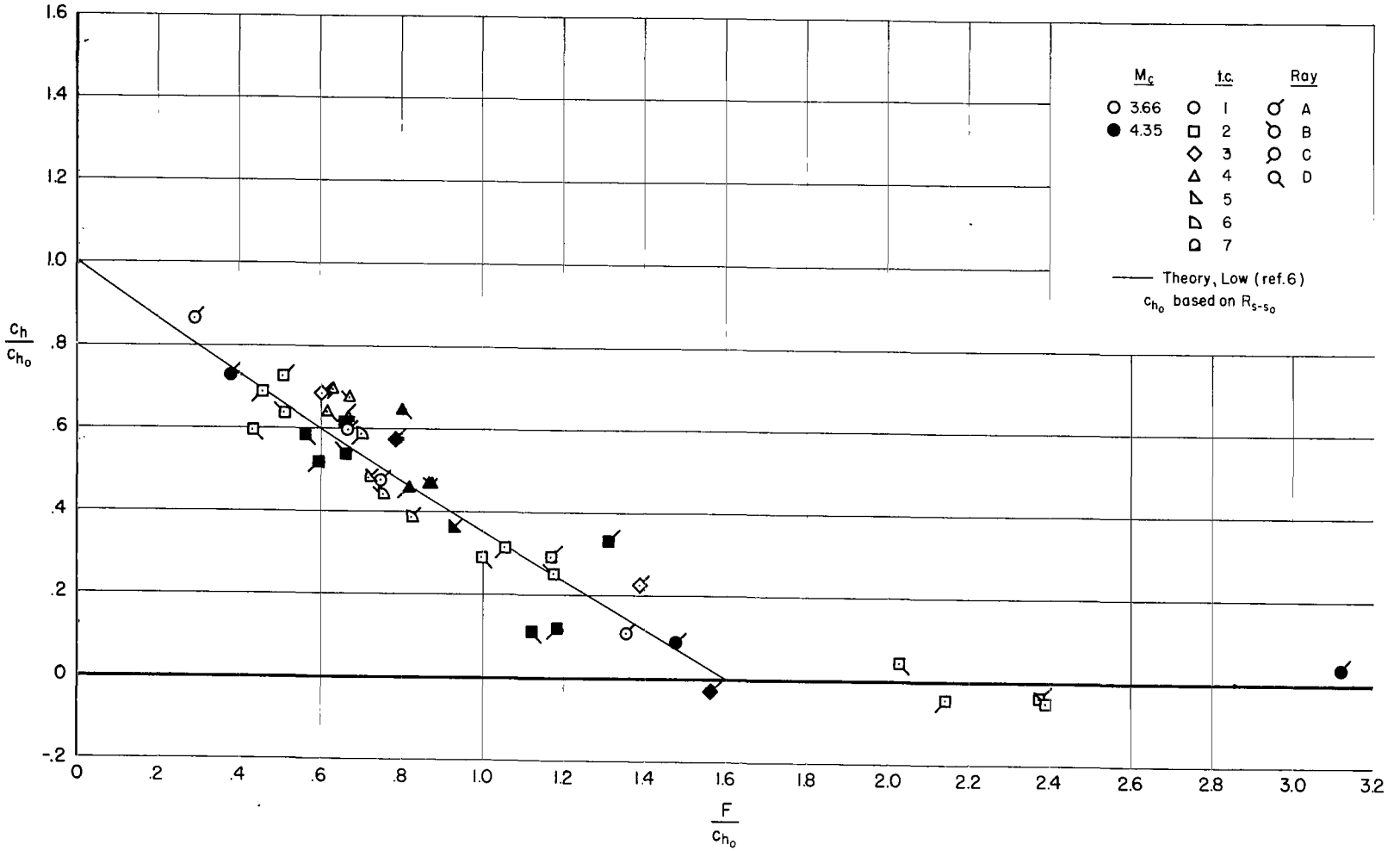

Figure 8.- Effect of mass transfer on Stanton number; air injection into laminar boundary layer.

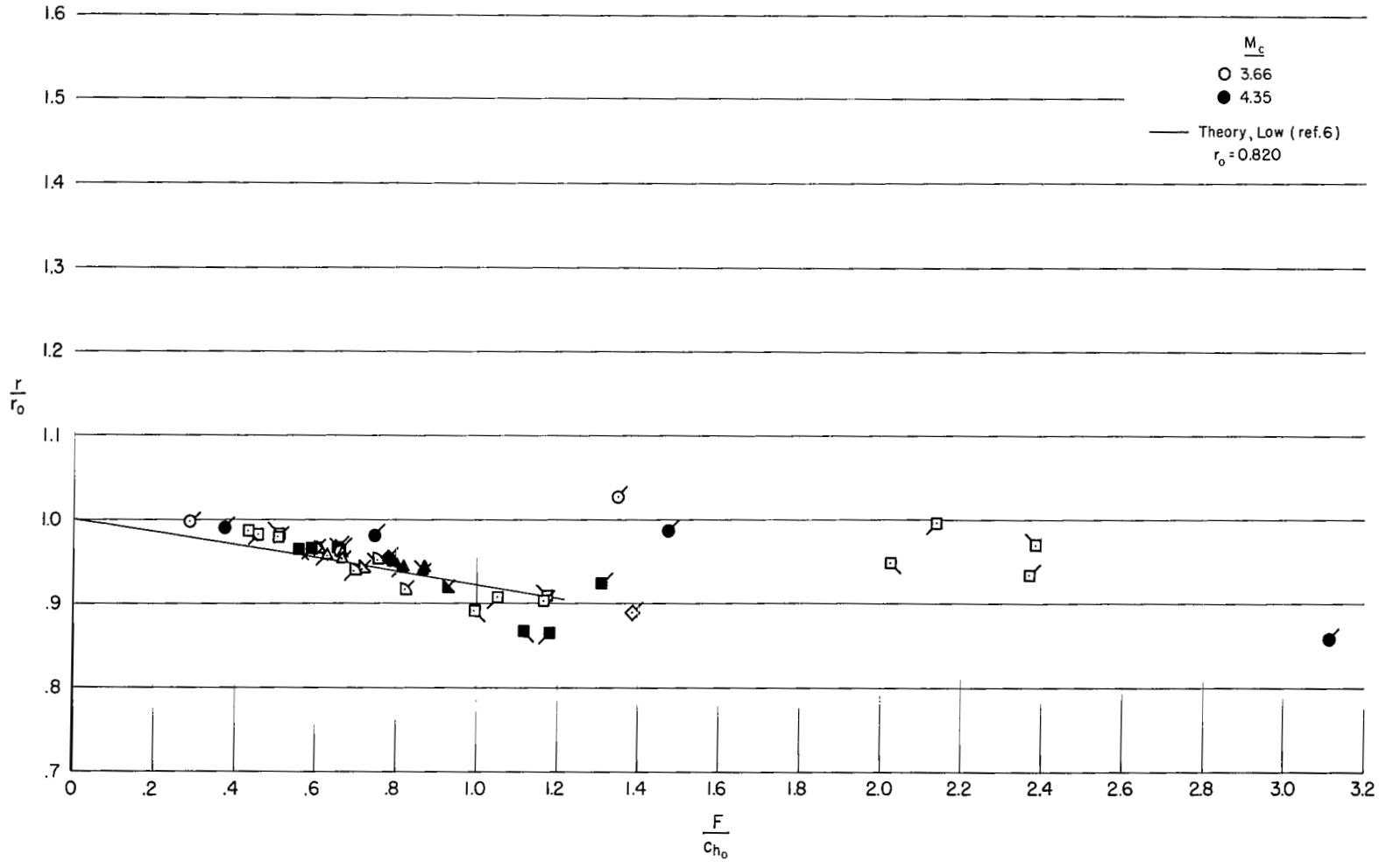

Figure 9.- Recovery factor with mass transfer; air injection into laminar boundary layer.

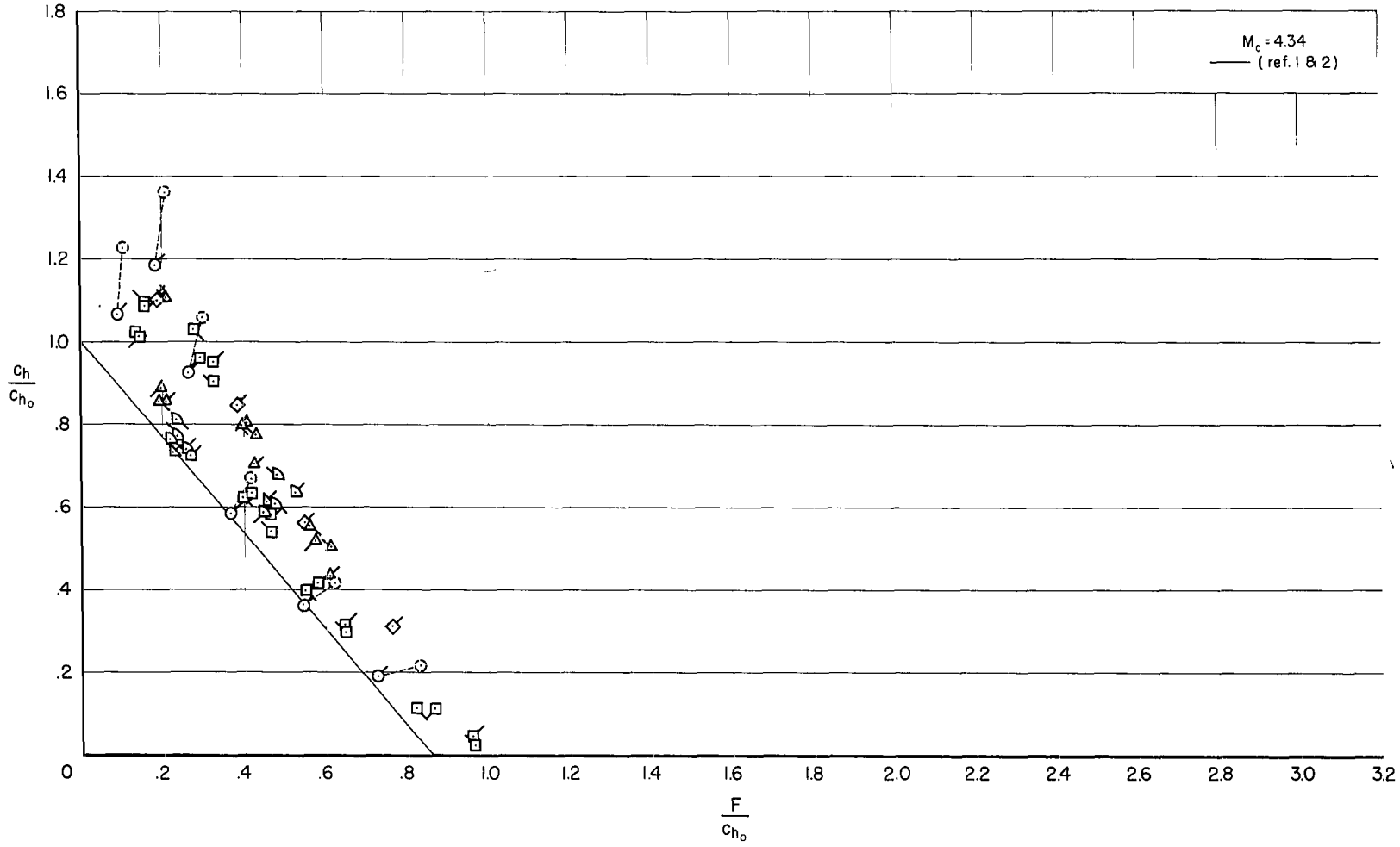

Figure 10.- Effect of mass transfer on Stanton number; helium injection into laminar boundary layer.

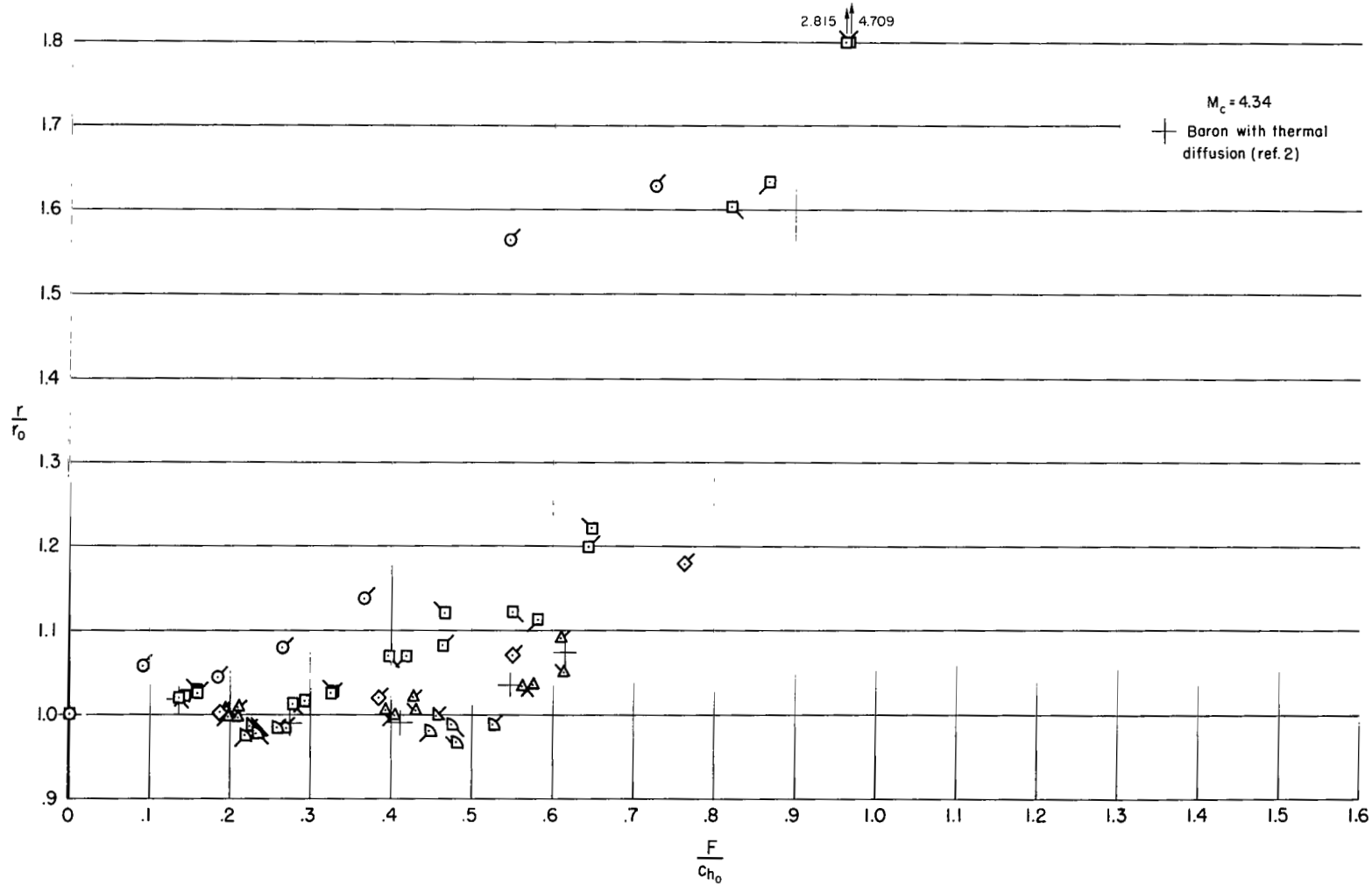

Figure 11.- Recovery factor with mass transfer; helium injection into laminar boundary layer.

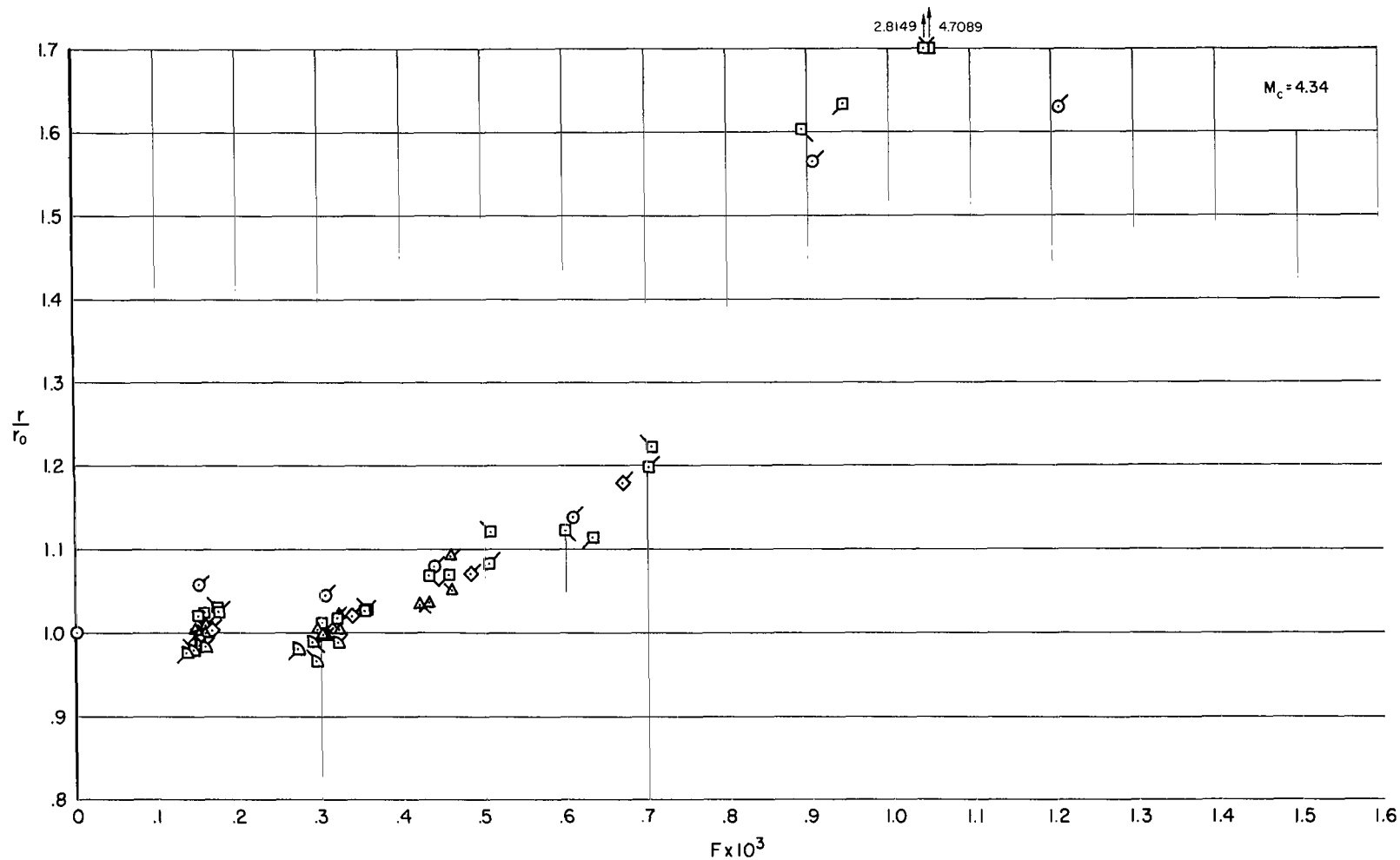

Figure 12.- Recovery factor with helium injection; alternative presentation.

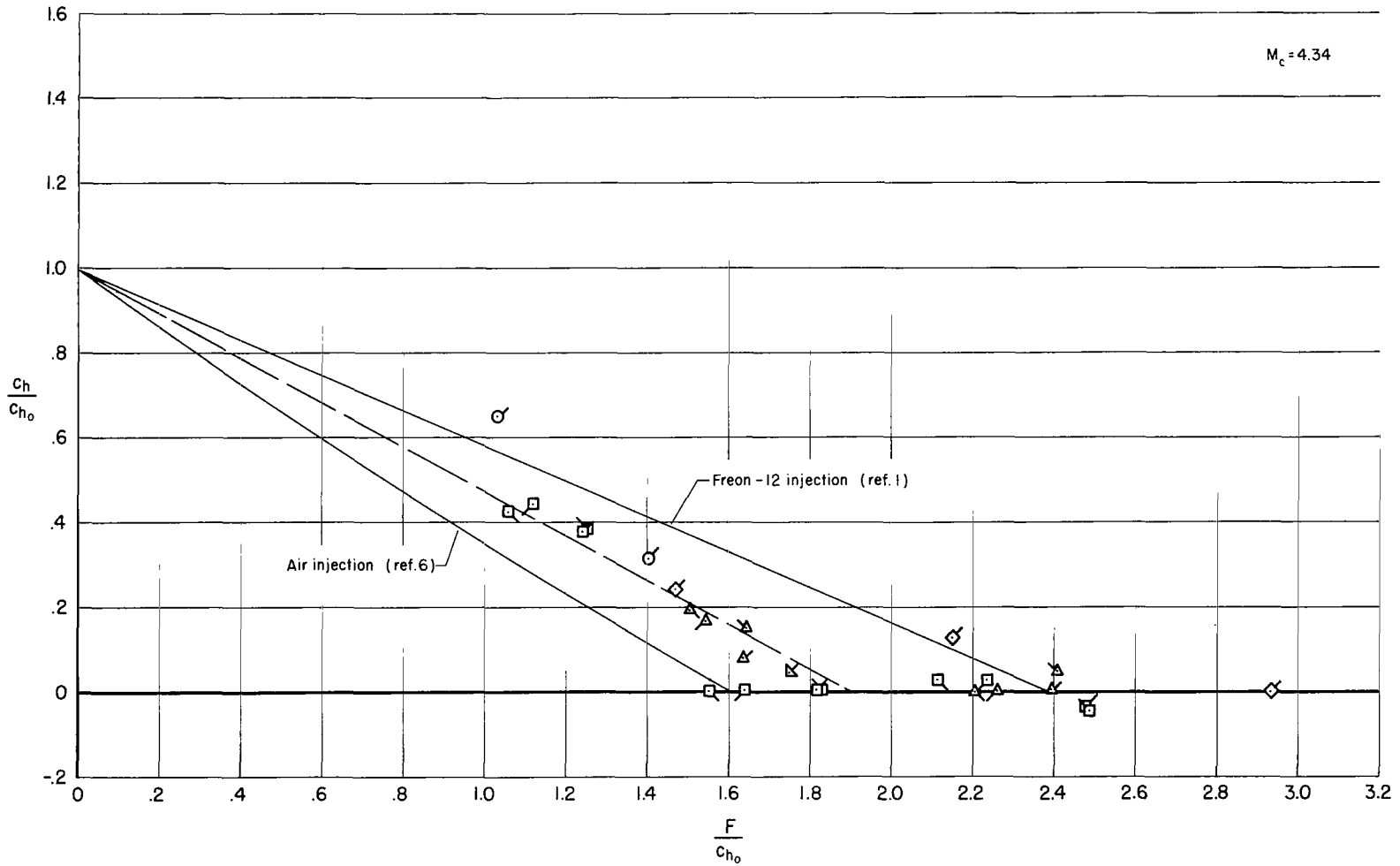

Figure 13.- Effect of mass transfer on Stanton number; Freon-12 injection into laminar boundary layer.

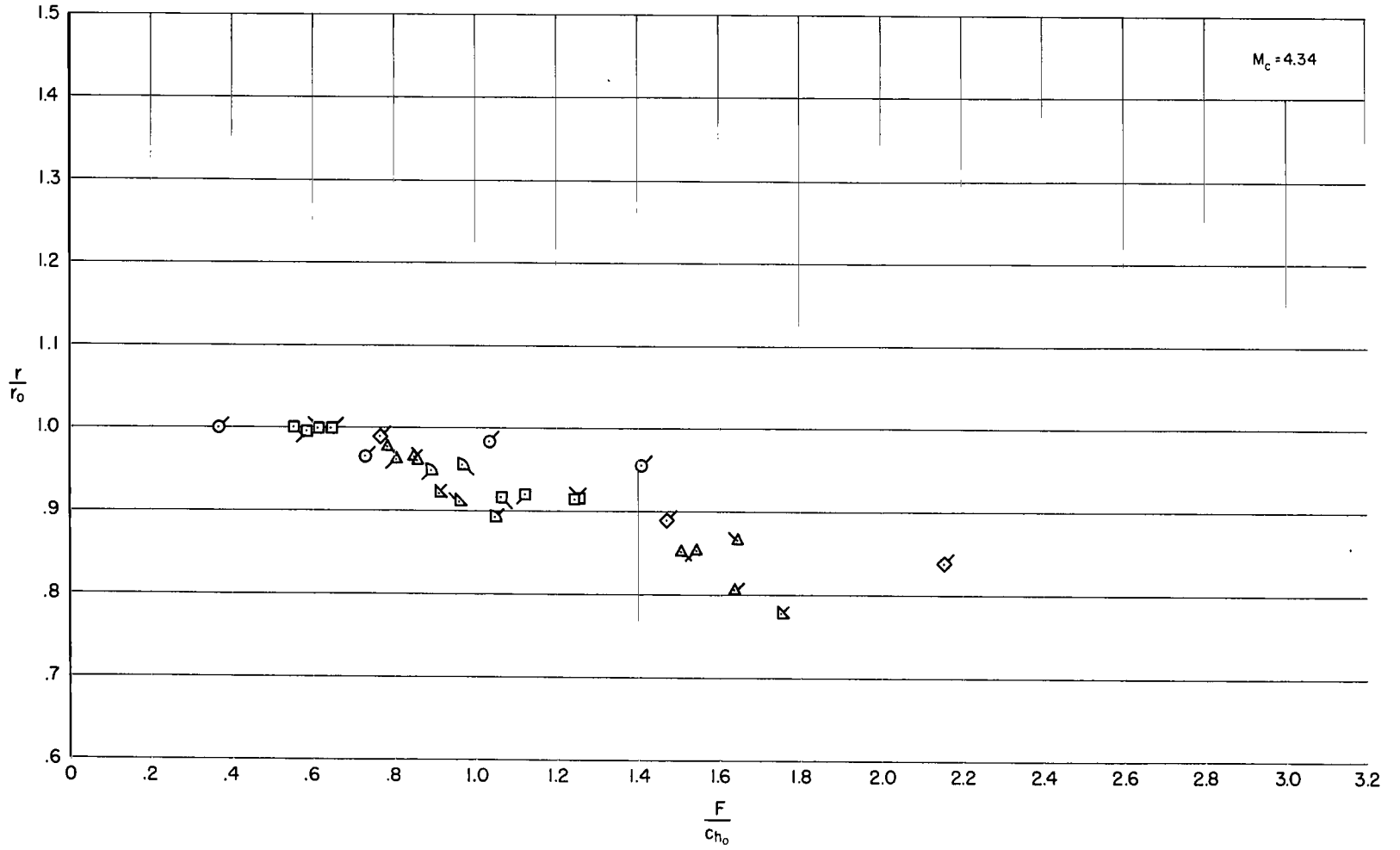

Figure 14.- Recovery factor with mass transfer; Freon-12 injection into laminar boundary layer.

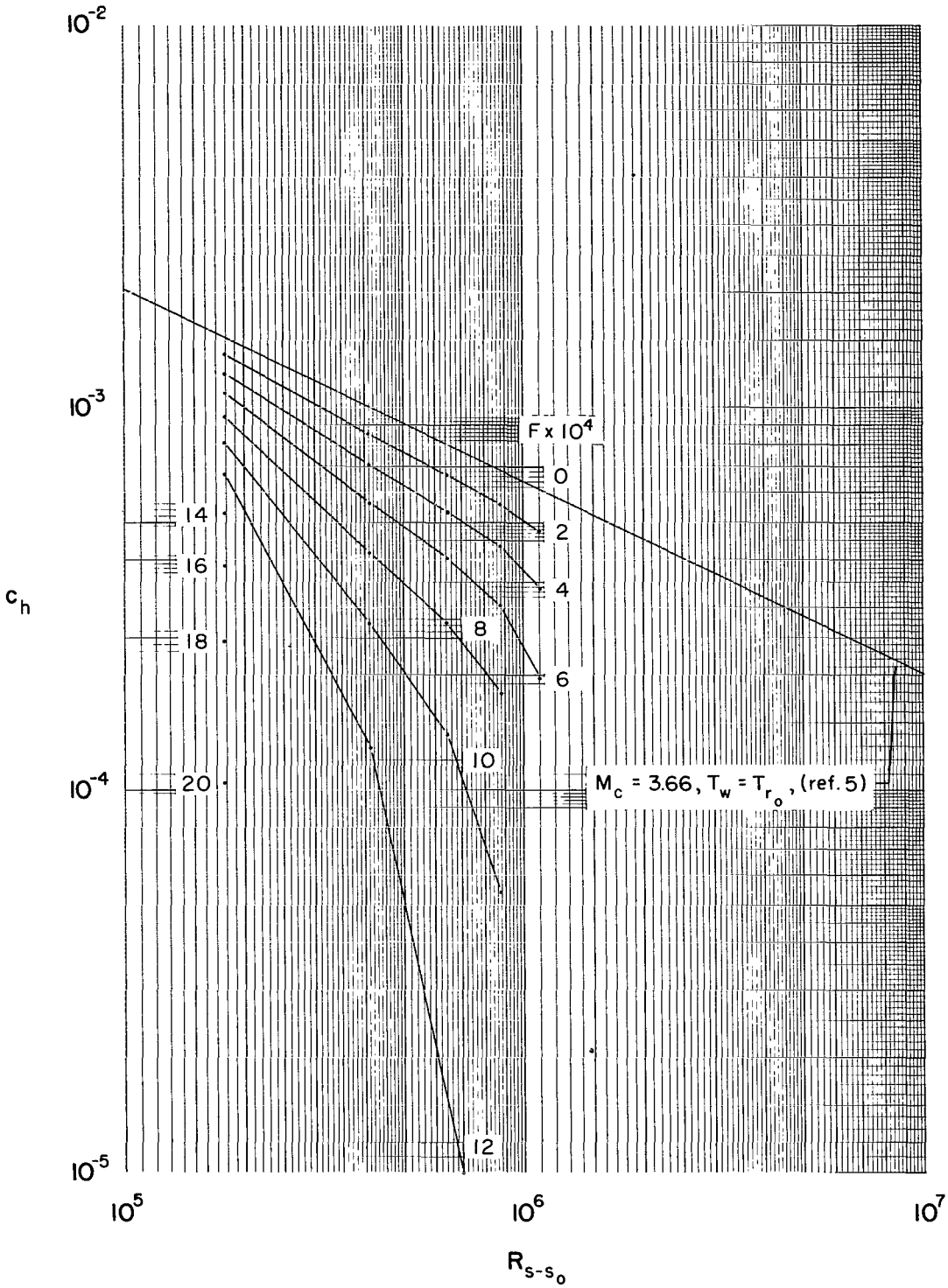

Figure 15.- Effect of air injection on local Stanton number on cone; laminar boundary layer.

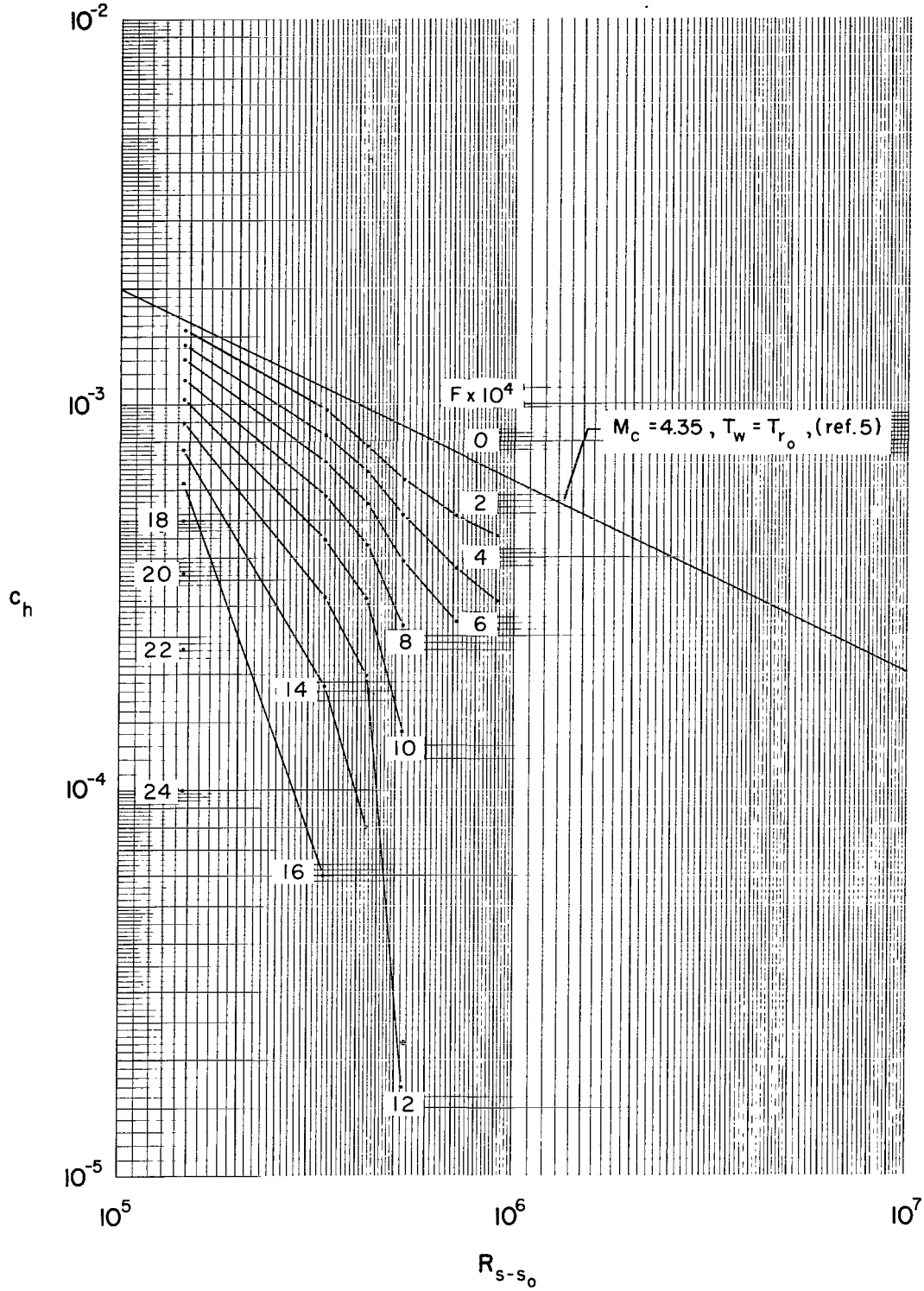

Figure 16.- Effect on air injection on local Stanton number on cone; laminar boundary layer.

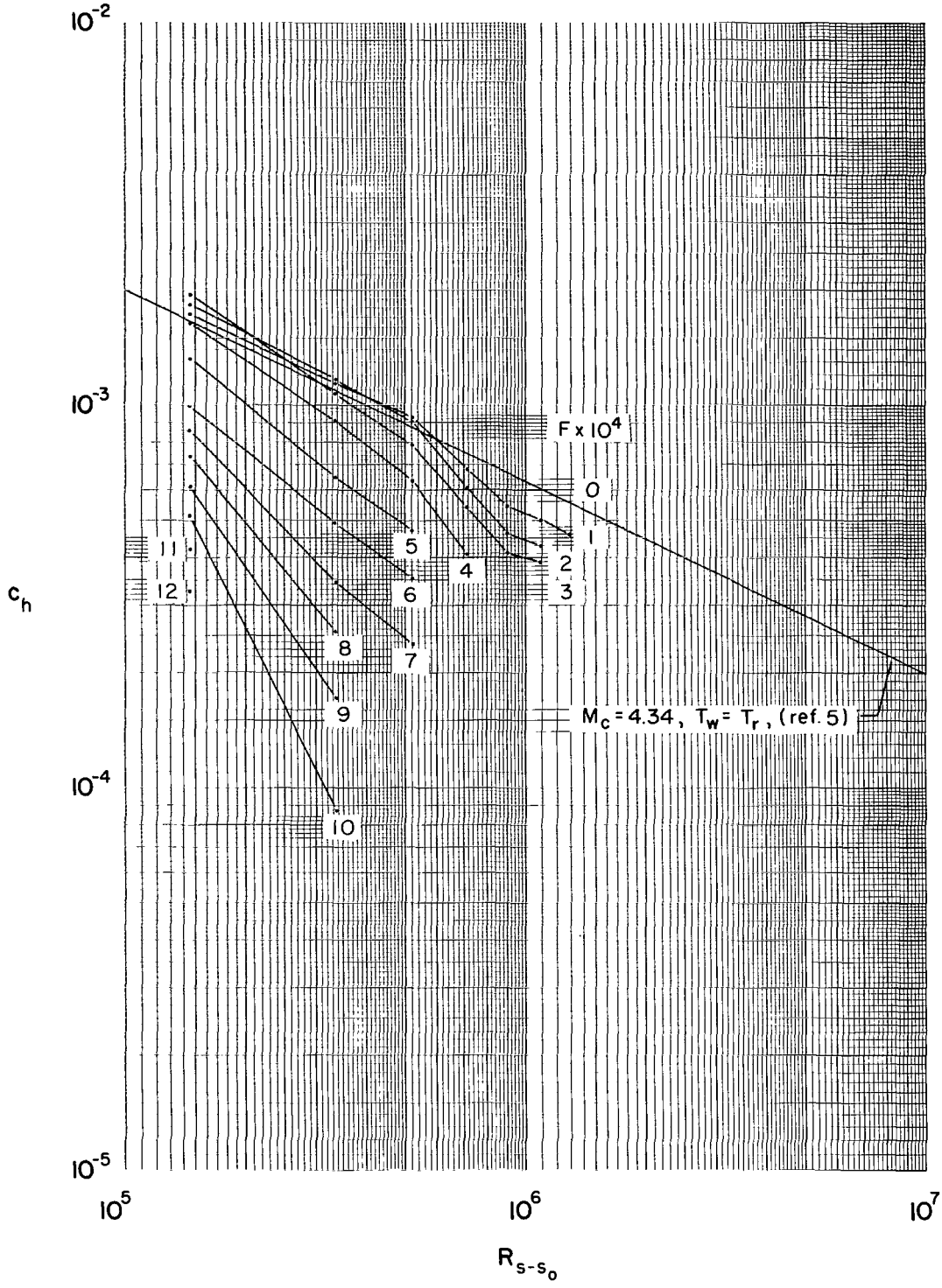

Figure 17.- Effect of helium injection on local Stanton number on cone; laminar boundary layer.

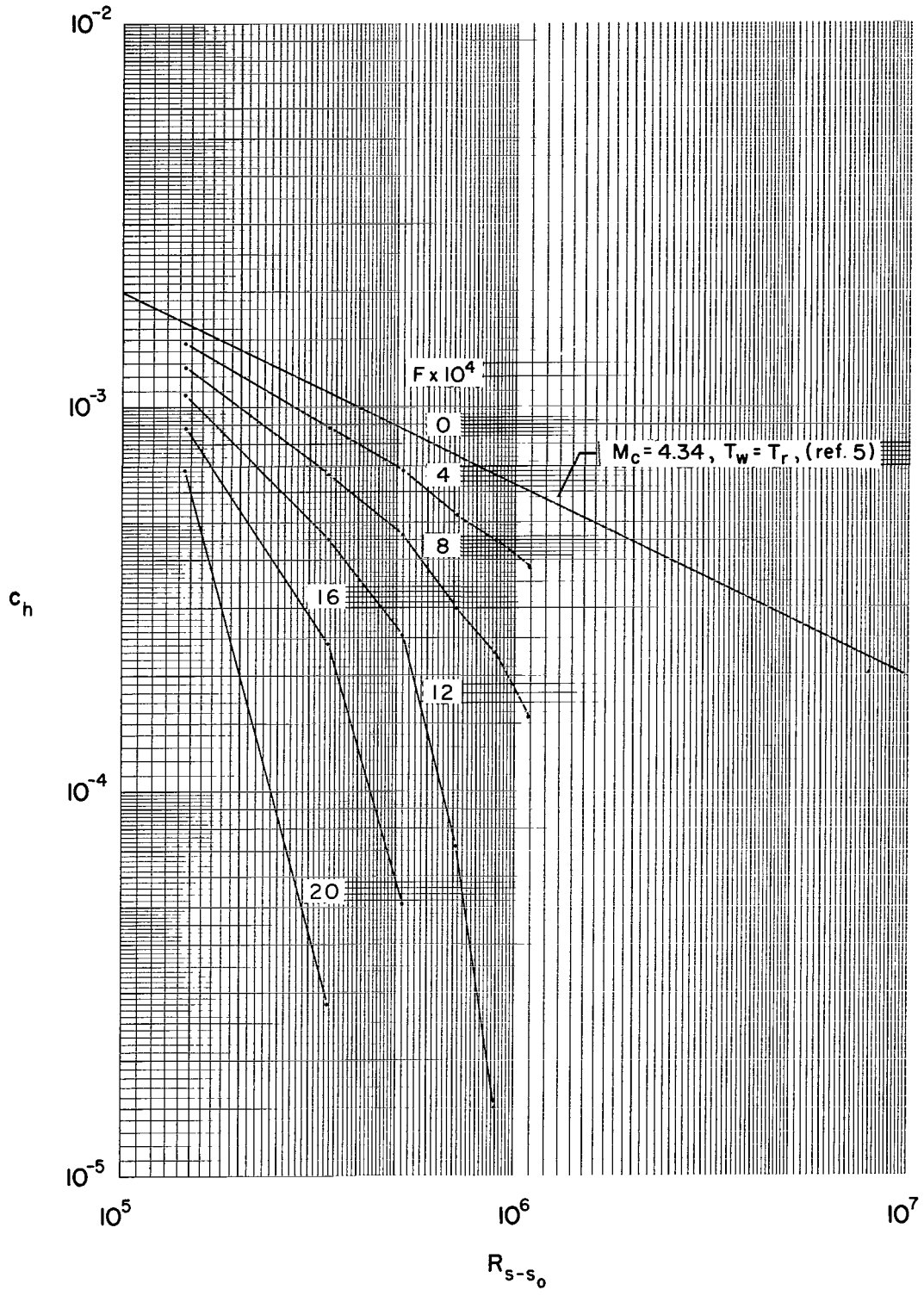

Figure 18.- Effect of Freon-12 injection on local Stanton number on cone; laminar boundary layer.

"The aeronautical and space activities of the United States shall be conducted so as to contribute . . . to the expansion of human knowledge of phenomena in the atmosphere and space. The Administration shall provide for the widest practicable and appropriate dissemination of information concerning its activities and the results thereof."

—NATIONAL AERONAUTICS AND SPACE ACT OF 1958

NASA SCIENTIFIC AND TECHNICAL PUBLICATIONS

TECHNICAL REPORTS: Scientific and technical information considered important, complete, and a lasting contribution to existing knowledge.

TECHNICAL NOTES: Information less broad in scope but nevertheless of importance as a contribution to existing knowledge.

TECHNICAL MEMORANDUMS: Information receiving limited distribution because of preliminary data, security classification, or other reasons.

CONTRACTOR REPORTS: Technical information generated in connection with a NASA contract or grant and released under NASA auspices.

TECHNICAL TRANSLATIONS: Information published in a foreign language considered to merit NASA distribution in English.

TECHNICAL REPRINTS: Information derived from NASA activities and initially published in the form of journal articles.

SPECIAL PUBLICATIONS: Information derived from or of value to NASA activities but not necessarily reporting the results of individual NASA-programmed scientific efforts. Publications include conference proceedings, monographs, data compilations, handbooks, sourcebooks, and special bibliographies.

Details on the availability of these publications may be obtained from:

SCIENTIFIC AND TECHNICAL INFORMATION DIVISION

NATIONAL AERONAUTICS AND SPACE ADMINISTRATION

Washington, D.C. 20546